NASA Technical Memorandum

NASA TM-86529

COMPUTED TOMOGRAPHY FOR NON-DESTRUCTIVE EVALUATION OF COMPOSITES: APPLICATIONS AND CORRELATIONS

By B. Goldberg, L. Hediger, and E. Noel

Materials and Processes Laboratory
Science and Engineering Directorate

August 1985

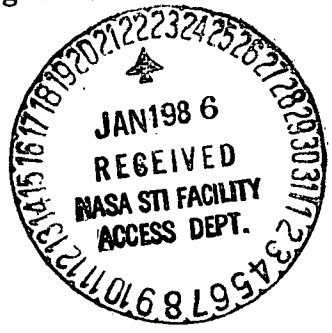

(NASA-TM-86529) COMPUTED TOMOGRAPHY FOR NON-DESTRUCTIVE EVALUATION OF COMPOSITES: APPLICATIONS AND CORRELATIONS (NASA) 51 p
HC A04/MF A01 CSCL 11D

N86-16268

Unclas
G3/24 05201

National Aeronautics and Space Administration

George C. Marshall Space Flight Center

TECHNICAL REPORT STANDARD TITLE PAGE

1. REPORT NO.	2. GOVERNMENT ACCESSION NO.	3. RECIPIENT'S CATALOG NO.
NASA TM-86529		

4. TITLE AND SUBTITLE	5. REPORT DATE
Computed Tomography for Non-Destructive Evaluation of Composites: Applications and Correlations	August 1985
	6. PERFORMING ORGANIZATION CODE
7. AUTHOR(S)	8. PERFORMING ORGANIZATION REPORT #
B. Goldberg, L. Hediger, and E. Noel	
9. PERFORMING ORGANIZATION NAME AND ADDRESS	10. WORK UNIT NO.
George C. Marshall Space Flight Center Marshall Space Flight Center, Alabama 35812	11. CONTRACT OR GRANT NO.
	13. TYPE OF REPORT & PERIOD COVERED
12. SPONSORING AGENCY NAME AND ADDRESS	Technical Memorandum
National Aeronautics and Space Administration Washington, D.C. 20546	14. SPONSORING AGENCY CODE

15. SUPPLEMENTARY NOTES

Prepared by Materials and Processes Laboratory, Science and Engineering Directorate.

16. ABSTRACT

The state-of-the-art fabrication techniques for composite materials are such that stringent species-specific acceptance criteria must be generated to insure product reliability. Non-destructive evaluation techniques including computed tomography (CT), x-ray radiography (RT), and ultrasonic scanning (UT) have been investigated and compared to determine their applicability and limitations to graphite epoxy, carbon-carbon, and carbon-phenolic materials. While the techniques appear complementary, CT is shown to provide significant, heretofore unattainable data. Finally, a correlation of NDE techniques to destructive analysis is presented.

ORIGINAL CONTAINS
COLOR ILLUSTRATIONS

17. KEY WORDS	18. DISTRIBUTION STATEMENT
Non-Destructive Evaluation Carbon Fiber Composites Computed Tomography	Unclassified — Unlimited

19. SECURITY CLASSIF. (of this report)	20. SECURITY CLASSIF. (of this page)	21. NO. OF PAGES	22. PRICE
Unclassified	Unclassified	50	NTIS

For sale by National Technical Information Service, Springfield, Virginia 22151

ORIGINAL CONTAINS
COLOR ILLUSTRATIONS

ACKNOWLEDGMENTS

The authors wish to acknowledge the contributions to Matthew Walker, III, who participated in data collection, analysis, and correlation on the GEBS program during a recent cooperative education assignment to MSFC. Mr. Walker is a student at the University of Tennessee in Knoxville.

TABLE OF CONTENTS

LIST OF ILLUSTRATIONS

LIST OF ILLUSTRATIONS (Concluded)

LIST OF TABLES

TECHNICAL MEMORANDUM

COMPUTED TOMOGRAPHY FOR NON-DESTRUCTIVE EVALUATION OF COMPOSITES: APPLICATIONS AND CORRELATIONS

I. INTRODUCTION

A. Background

This report defines the status of the MSFC Computed Tomography (CT) research efforts. CT, a tool developed to augment x-ray systems, has recently been investigated to determine its limits and capabilities for non-destructive evaluation of materials [1,2]. Prior to a discussion of CT principles and research, a brief historical review is presented.

The principles of mathematical image reconstruction were described as far back as 1917 by the Austrian mathematician J. Radon while working on equations involving gravitational fields; the use of such techniques for imaging tools took somewhat longer to evolve.

In the early 1960's, D. C. Kuhl and R. Q. Edwards developed a transmission tomography system using simplistic reconstruction techniques; the resultant images were somewhat distorted [3]. Throughout the 1960's, many other prototype CT systems were designed and built. However, image reconstruction, though improved, required considerable time. These state-of-the-art problems promoted development of faster, improved systems.

Advances in computer technology in the 1960's led to the production of the first generation of commercially available CT scanners where the x-ray source and the detector rotate synchronously around the object. A second generation of CT instruments was introduced in 1974; it utilized a fan-shaped array of multiple x-ray beams. With this configuration, data collection times were reduced to as little as 20 sec, and then to 5.3 sec [3]. Reduction in scan time remained a driver for CT optimization and, third and fourth generation CT systems were developed during the 1970's.

The historical review reveals that the development of the CT procedure was tailored for medical concerns. However, the generic nature of the tool promotes usage for varied applications.

CT combines computer technology and more traditional forms of x-ray transmission measurement to produce a cross-sectional image resulting from the mathematical reconstruction of measurements obtained when the x-rays are passed through a test object. There are three basic components in any CT scanner (Fig. 1). The first is a data collection system which includes an x-ray source and accompanying gantry, a parts manipulator, and an array of detectors to receive the transmitted x-rays. Photodiodes are the most widely used detectors in industrial CT scanners, though photomultipliers are also used [4].

The collected data must be stored and processed to produce the image. This requires a computer, the second major component of the CT scanner. Finally, the mathematically reconstructed image from the computer is displayed on a view console, the third major element.

To obtain a completed CT scan of a single slice through the test object, thousands of measurements must be collected of the transmitted x-ray beam. As the x-rays are transmitted, they are attenuated; therefore, accurate reconstruction of the image requires specific attenuation compensation.

The data processor divides the volume of each slice into basic units called picture elements, or pixels; the average amount of attenuation across each pixel volume is recorded. This attenuation information is then converted into units termed CT numbers. The CT number of a material is related to the linear attenuation coefficient, μ, of the material for the specific effective energy of the x-ray beam:

$$\text{CT number} = K \frac{\mu - \mu_w}{\mu_w}$$

where μ_w is the linear attenuation coefficient of water at the same effective energy; K is a constant which has the value of 1000. CT numbers are referred to as Hounsfield units (HU). The HU expression is

$$HU = 1{,}000 \frac{\mu - \mu_w}{\mu_w}$$

In HU, air has a value of -1000, water is 0, and high density metals range as high as 1000 [4].

After completion of calculation of CT numbers for each pixel of the slice, a matrix of all the numbers is arranged, each again corresponding to an average density across each pixel. The image is then reconstructed by converting each CT number within the matrix into a grey-scale (or color) image. This reconstructed composite grey-scale image is displayed on a viewing console, and additional enhancement is limited only by the systems capabilities.

B. Concerns Investigated

Three distinct types of composite materials have been examined with CT to determine the applicability of the evaluation technique for the material. The material systems, their usage potential/requirements and problems are detailed below:

1. Graphite Epoxy

Efforts aimed at reduction of weight of the Space Shuttle and consequent increased mission cost effectivity have resulted in examinations of usage and applicability of high strength, light-weight composite materials. Among these is graphite epoxy.

Graphite epoxy materials are particularly sensitive to moisture absorption, primarily due to the high affinity of the epoxy compounds for water. The degradative

effects of moisture absorption are also aggravated by elevated temperatures. Matrix-dependent properties, such as flexural, shear, and compressive strengths are the most sensitive to this degradation. Fiber dependent properties, such as tensile strength, are far less affected, even by these adverse environments [5].

Since a moisture-controlled environment is difficult to maintain throughout an effective test program, initial MSFC investigations with graphite epoxy were for high-tensile strength applications. Among these are the graphite epoxy filament-wound bipod struts (GEBS) currently being assessed for the application to both forward and aft Orbiter-to-External Tank (ET) attachments.

The graphite epoxy investigation goals were two-fold: determination of optimum NDE techniques and applicability of these techniques to failure prediction and acceptance criteria. As no preliminary stress analysis or critical materials properties data were delineated, a complete mapping of all NDE locations was performed.

Six struts, fabricated by Engineering Technologies Corporation, were investigated by NDE techniques. The limitations of each NDE technique eliminated accurate determination of part-specific quality by any singular method. However, correlation of NDE data from several techniques was assessed to determine if it provided a medium for determination of relative probabilities of failure. These correlation efforts will be detailed herein.

2. Carbon-Carbon and Carbon-Phenolic

The fabrication and acceptance methodologies for carbon-carbon materials have recently been shown to be inadequate for flight usage in Payload Assist Module (PAM-D) exit cones [6]. The problems, while manifested catastrophically only for STAR 48 cones on PALAPA-B2 and WESTAR-VI missions, are present throughout the exit cone fabrication industry. The utilization of "experience derived" proprietary steps for cone fabrication, rather than firm scientific method-based process understanding is currently being addressed through several NASA contracted efforts. The understanding of non-destructive testing methodology and associated correlation of results to performance, and thereby component acceptance, provide an equally challenging research venue.

The failure investigation for the PALAPA and WESTAR mission lead to initial review and preliminary development of CT scanning for carbon-carbon materials. The fabrication technique for the PAM type exit cones (called involute cones) involves circumferential lay-up of numerous plys in a rosette structure. This carbon-phenolic billet is then cured, pyrolized to remove the resin matrix, and reimpregnated using a carbon-vapor-deposition (CVD) process. While the final results of the impregnation process are tested for strength, it is clear that these techniques result in a material with variable density. The CVD process inherently leads to a carbon skin formation on the cone exterior and, in conjunction with the relative uniformity of the pyrolization process, heterogeneous dispersion of the carbon impregnant. CT scanning has been demonstrated to display these density variations and reveal excessively matrix-poor planar regions that may form interply. One study has concluded that these dry ply regions provide a weak link in the exit cone, leading to potential failure through a cross-ply tensile failure mode. However, to date, little work has been accomplished to correlate the CT images to tangential and radial x-ray data. The results of examinations contained herein pertain to this type of correlation effort rather than that associated with exit cone acceptance criteria.

The cone selected for this research was fabricated by HITCO and designated SN 30195. This cone was selected for CCT-1, an MSFC directed 10-sec sea-level firing at Morton Thiokol-Elkton. The cone had been x-rayed and CT scanned as an exit cone and x-rayed as both an exit cone assembly and nozzle assembly prior to the firing. The highly instrumented nozzle assembly was then fired in ground test. The results of this test are published elsewhere [7]. The PAM-D portion of the MSFC CT work represents the investigation and correlation of post-fire x-ray, CT, and visual observation efforts.

The carbon-carbon type material is used as a heat radiator type exit cone; a second major type of composite exit cone material, one that ablates, is also used. The ablators include carbon-phenolic materials. While erosion characteristics of fired components are easily determined, the range of heat-affected zones present in ablative components is currently subject to experimenter sensitivity. Carbon-phenolic will form char layers and heat affected zones; these regions will vary in density. Previous efforts for mapping these regions involved insertion of a proble until, by feel and alcohol evaporation technique, a zone depth was determined. The subjectivity of this procedure, combined with non-homogeneous density variations, provided for inconsistent thermal characterization. This report will detail the investigation of these density regions using the CT technique.

II. EXPERIMENTAL PROCEDURES

Experimental procedures may be divided into four major categories: ultrasonics, radiography, computed tomography, and mapping.

A. Ultrasonics

Through-transmission emergent ultrasonic evaluation was performed for two materials using a Testech system designed for MSFC. Ultrasonic evaluation procedures were developed for specific sample requirements. The instrumentation settings are detailed in Table 1 for the carbon-carbon exit cone material and the graphite-epoxy bipod strut material.

B. Computed Tomography

Computed Tomography was performed during each of the investigations using an ELSCINT model 2002 medical CT unit. In addition, a GE 9800 CT unit was used for the CCT-2 investigation with MSFC facilities employed for image resolution. All investigations required 140 KeV and 40 mA with a 512 x 512 pixel reconstruction matrix. The procedures developed for each investigation are detailed in Table 2.

C. Radiography

Radiography was performed during each of the four investigations using a Phillips 320 KV x-ray head. The procedures developed for each application are detailed in Table 3.

D. Mapping

Three techniques were employed for mapping the accumulated NDE location data:

a) Visual data recording: Visual data were mapped on fold-out surface maps developed for each application.

b) Anomaly profiling: A three-dimensional view of each anomaly was approximated by creation of a map of stacked sequential views. This technique was especially useful for mapping anomalies detected by tangential radiography and computed tomography.

c) Comparative analysis/data correlation: Data taken by each NDE method was mapped separately. These maps were compared to each other and correlations noted. The correlations were then assembled into a final data correlation map. This technique required the usage of computer-aided interactive color graphics.

A summary of data mapping techniques is presented in Table 4.

IV. RESULTS/CONCLUSIONS

A. Graphite Epoxy Bipod Struts

The GEBS program required NDE predictions for the performance of each strut under tensile loading conditions (Fig. 2). The NDE assessment was based on relative probabilities of failure generated by correlation of NDE determined anomalies. Three methods, ultrasonic inspection (UT), radiographic inspection (RT), and computed tomography (CT) were used for the three phase procedure comprising raw data analysis, mapping, and quantification.

Several types of anomalies were characterized during the raw data analysis procedure. Data was then mapped and cross-referenced by location in an attempt to profile the anomalies. Anomaly profiles were then transferred to a separate map comprising quantifiable data for each strut. These quantifiable data contained the resolved anomaly types of delamination, delamination-like region (including high void content regions) and resin-rich/resin-starved area.

Relative probabilities of failure were calculated for each strut based on the extent of the quantified anomalies. These conditions were resolved as the area of the region parallel to the sample surface. The approach chosen was to quantify the extent of the conditions as a percentage of the delamination-type region (Appendix A).

The second goal of the GEBS assessment was the determination of the applicability of CT to graphite epoxy components. CT data was found to provide more meaningful information than tangential RT data (Figs. 3 and 4). CT provided data taken over the entirety of the object as opposed to RT selective angular location approach and data with superior contrast and clarity to RT data. Further, CT appears to be less directionally sensitive than RT.

Correlation of CT to the other two methods also provided information as to the current limitations of the technique. While void content and density gradients proved more easily resolved through CT, delaminations detected by UT were extremely

difficult to locate with CT (Fig. 5). In most cases, delamination detection proved impossible. Further testing on GEBS segments indicated that CT was not a reliable detector even for visible delaminations (Fig. 6). RT was only slightly more useful in detecting delaminations.

The dissimilarity in attenuative behavior of the graphite and the epoxy components may prevent detection of sharp details in this material. These problems may be overcome by tooling improvements or usage of a higher energy source. The use of CT for thin shelled objects has been known to be problematic; the placement of a tight fitting silicon plug inside the GEBS structure served to sharpen some details.

B. Carbon-Carbon

After the ground test firing of CCT-1, the exit cone assembly was examined (Fig. 7). Data from three non-destructive techniques was accumulated and analyzed (Table 5).

Axial x-ray data from the exit cone assembly was clearly technique limited as to the information that was obtained. While the clarity of Figure 8 is less than that of the x-ray film, several features are discernible:

1) Instrumentation: Including pressure transducers, thermocouples and strain gauges.

2) Zinc chromate putty: Char and virgin (innermost ring at quadrature).

3) White circles identifying anomalous NDE indications.

Resolution of the above indications was possible using the x-ray film. Regions of large bond gap (carbon-phenolic to carbon-carbon), potential hot gas flow and density variation were noted (Fig. 8).

Tangential x-ray slices were also examined to determine bond-gap, o-ring effectivity, and cracks/anomalous deviations within the exit cone assembly components (Figs. 9, 10, and 11). Again, the clarity of Figures 9 and 10 is less than that of the x-ray film. However, the variation in both the bond gap and o-ring free volumes, while not measurable, may be discerned from these figures.

The indications from the tangential x-ray data were mapped and their axial locations measured (Fig. 11). These data were then plotted on axial slice maps in an attempt to correlate these data to CT data.

The CT data on the exit cone assembly provided information delineating the suitability and limitations of the CT technique to exit cone assemblies. The STAR 48 assembly has a titanium ring attach fitting on the exterior of the carbon phenolic insulator (Fig. 7). The high density of this ring caused high scattering and anomalous indications in the slices resolved at its location (Fig. 12).

However, the CT data was superior for determination of the bond gap between the carbon-phenolic and carbon-carbon components (Fig. 13). It may be seen from these figures that the gap is circumferentially non-uniform. Further, it is apparent from Figure 13 that a region of flow or "erosion" is located at the 20 deg position

(0 deg at 12 o'clock, incremented clockwise). The regions of low density in the interior of the slice are bubbles in the CT fixture and, for the purposes of this investigation, are meaningless.

A somewhat less clear indication of the non-uniformity of the bond gap is visible farther down the assembly [Fig. 14(a)]. It must be noted that, as was the case for the x-ray data, the figures display less clarity than the CT data. Finally, a display of the strobing effects caused by high density objects is presented [Fig. 14(b)].

The results of the correlation effort for CT and x-ray data are presented (Fig. 15). While the x-ray technique for transfer of tangential indications to axial slices is tedious and labor-intensive, the CT indications are found to be in excellent agreement. Further, it may be seen that the two techniques are not redundant, but rather complementary. The x-ray indicates a region of potential flow not noted on the CT. After this indication was determined, a reinvestigation of the CT did reveal a slight anomaly at the cited location. However, as this investigation was centered upon correlation of initial indications, determined through distinct methods, these data were not included in the correlation maps. CT was able to delineate planar locations that the x-ray was unable to resolve. Finally, although both techniques were able to resolve the presence of the instrumentation, the x-ray method provided additional information on the exact location of the high density probes.

The final portion of the CCT-1 NDE effort was a correlation of the NDE data to destructive evaluation. Figures 16 and 17, taken by Morton Thiokol/Elkton Division during nozzle dissection, indicate that the correlation is quite good. Figure 16, representing the forward section of the exit cone assembly, reveals that:

1) The o-ring gap is not circumferentially uniform and is in excellent agreement with the distribution resolved throughout the NDE effort.

2) The bond gap in the thread region appears to have varying amounts of adhesive; again in excellent agreement with the CT data.

3) The exit cone has shifted axially with respect to the insulator. CT data indicates a potential for a slight cocking of the cone.

Figures 17(a) and (b), of the aft section of the exit cone assembly, indicate the instrumentation and slight variation in bond gap thickness. This variation is slight and finer resolution is achieved through implementation of the CT technique.

As an addendum, at the time of this publication the results from a second ground firing, CCT-2 are under review. Pre- and post-test CT data was taken of the exit cone assembly which proves the theoretical "cocking of the exit cone assembly" presented above (Fig. 18). This data will be presented in a follow-on report.

In another attempt to determine the significance of NDE indications, an aft section of the CCT-1 exit cone was examined through x-ray and ultrasonic techniques. The section, 16 in. in axial length, was instrumented with strain gauges and acoustic emission sensors (Fig. 19). The section was then hydrobuckled. A report of this effort has been presented detailing the strain and stress analysis [8].

The hydrobuckled section was evaluated with visual, x-ray and ultrasonic techniques. A complete mapping of these data are presented (Fig. 20). The green indications are the regions of high attenuation located through ultrasonic inspection pretest. The straight black lines located between 200 and 260 deg are the x-ray indications typically termed planar indications. The two black dots at 210 and 240 deg are x-ray indications for a high density inclusion and a missing fiber region, respectively. The circles represent the acoustic emission data taken during the test. The blue regions in Figure 20 represent the visual observations post-test (Fig. 21). The regions at 20 deg, above and below the stiffener ring, the regions at the sites of the x-ray indications (210 and 240 deg), and the small region at 250 deg represent regions in which surface indications came into being post-test. These surface markings were either cracks/surface crazing indications (locations at 20 and 250 deg), or surface discolorations (locations at 210 and 240 deg).

The correlation of the pre-test maps with the visually observed post-test indications provides several clear evaluation results:

1) The ultrasonic emission regions of high attenuation, while in reasonable agreement with the acoustic emission measurements (recorded during test), do not seem to directly correlate with visual observations of post-test indications.

2) The pre-test x-ray indications provided a clear determination of the failure points. Further, the x-ray indications that were not of the planar void type were correlatable to post-test visual surface indications.

Microscopic evaluation of the surface and failure site indications was performed (Figs. 22 and 23). The evaluation of the regions indicated that:

1) The regions defined as dry ply by the pre-test x-ray evaluation appear to have less matrix material and a higher incidence of "clean" fiber bundle visibility.

2) The surface indications are quite shallow and appear to indicate localized regions of high residual strain.

The post-test evaluation of the x-ray data did not reveal the indications defined by the pre-test efforts. Subsequent inspection by ultrasonic techniques revealed that the average attenuation (and inversely corresponding density) had risen (or lowered). It appeared that the x-ray indications were not visible due to the general lowering of the average density of the entire sample. This degradation of the material may well be due to microcracking during the test. Further investigation is clearly warranted.

C. Carbon-Phenolic

1. Solid Rocket Motor

Six SRM segments were inspected, three fired and three unfired (Fig. 24). The segments had been machined from several component rings of actual SRM nozzle assemblies. Preliminary radiographs of the segments were also received from the MSFC Reliability and Quality Assurance Office.

Analysis of these preliminary radiographs and concurrent visual inspection of the fired components indicated that, with the exception of CT, additional NDE was not required. The radiographs of these segments readily disclosed the charring and

delaminations noted through the visual inspection (Fig. 25). Thermal cracking was evident in two of the fired segments. Cloth-to-cloth lacing patterns were visible in one of the fired segments. Tangential radiographs of the fired segments also indicated that the char/erosion profile ranged from 20 percent (in the thickest segment) to 100 percent (thinnest segment). More subtle anomalies may have been masked by these conditions. The complex geometry of char and erosion patterns prohibited successful ultrasonic inspection.

The initial radiographs fo the unfired segments disclosed slight film-density changes which were correlated to visible cloth patterns and cloth-to-cloth lacing patterns in the segments. Several other film patterns were traced to visible surface conditions. Uniform light and dark bands which ran the entire length of the segments were initially attributed to sample geometry effects. Finally, several slight film-density variations were noted. Additional radiographs of the unfired segments, taken in radial and true tangential planes, were examined to investigate these anomalies (Figs. 26, 27, and 28).

These radiographs eliminated the ply-to-ply superpositioning effects that were evidenced in the initial radiographs. However, the radiography technique remained limited by the complex part geometries; the light/dark banding problems were not eliminated.

Radiographs of each of the unfired segments were mapped to determine correlations with CT data. Detailed surview sketches, identifying the precise location of desired CT slices served as a guide for the tangential direction CT inspection (Fig. 29). In all the segments, several uniform low-density/high-density bands, parallel to the ply lay-up direction were noted (Fig. 30). The density variation present in these bands ranged from 10 to 20 percent (low density, 1.2 g/cc; high density, 1.5 g/cc). These bands may result from the compaction and resin flow procedures present during the cure cycle.

In addition, several non-uniform variable density regions, presumed due to resin flow variability, were located. One such indication was profiled throughout all the slices investigated. This indication was also noted through visual, standard radiographic, and axial CT inspections (Figs. 24, 25, and 31).

Axial CT was performed on both the fired and unfired segments. Axial CT of the unfired segments corroborated the variable density bands noted during the tangential CT investigation. In addition, axial CT provided information on both the depth and extent of the indications. Axial CT of the fired segments confirmed the depth of char/erosion pockets seen in tangential RT, as well as the depth and extent of delaminations.

In an attempt to correlate ultrasonic inspection with the CT and radiographic data, both the fired and unfired segments were inspected. The combination of complex part geometries and couplant concerns proved prohibitively severe; no meaningful data was acquired with this technique.

CT clearly provided information concerning the location of regions affected by cure variation, the depth and extent of delaminations, and the depth and extent of char/erosion regions. At the time of publication of this report, destructive analysis of the cited segments is ongoing in an investigation aimed at correlation of NDE data to destructive data. These results will be published at a later date.

2. Char Profile

As the current techniques for determination of char and heat affected regions in carbon-phenolic exit cones are subjective and operator sensitive, CT was used to examine sections from two ground test firings: NQ1 and NQ2. These sections had been mapped for char and heat affected regions by the standard techniques, and the variability in results was extremely high.

Investigation with CT revealed not only a non-subjective char and heat affect region profile, but an explanation for the variability of the operator subjective method heretofore employed. Figures 32 and 33 are CT slices from the NQ2 exit cone segments. The thicker sections (Fig. 32) clearly reveal numerous density layers. Detailed examination of the CT images indicated that the char layer — innermost on the cone ID — was separated from the remainder of the exit cone by a lower density region. This region may be explained by the thermal expansion properties of the composite.

As the composite exit cone is heated during the firing, several regions are created. These temperature sensitive regions are caused by the thermal degradation of the phenolic resin. The innermost region will be char, with successively less heat-affected regions found radially through the sample. As these regions cool, it is apparent that the differing coefficients of thermal expansion will tend to separate the sections. While cool down cracks have been noted, no one has related this phenomenon to the char profile effort.

CT investigation reveals that there are several regions of microvoids and microcracks between the various regions delineating distinct degrees of heat affect. Even the aft sections (Fig. 33) display these regions. Mapping the char and heat affect regions is no longer subject to revision nor subjectivity. It is considered that this work will provide the basis for implementation of CT scanning of carbon phenolic materials as the standard technique for char/heat affect region mapping in the future.

IV. SUMMARY

The techniques presented have been shown to be complementary. UT serves as an optimum discriminator for determination of delaminations in graphite epoxy composites, RT permits profiling precise location of high-density nozzle instrumentation, and CT provides heretofore unavailable data for char line determination. This investigation has served to provide additional emphasis for research with the CT technique. While older techniques have been somewhat refined for composite materials applications, CT has yet to be optimized. Though a relatively new technique for NDE, the application of CT has been clearly demonstrated. Further research is clearly warranted for correlation of NDE anomaly indications to mechanical properties and process control.

REFERENCES

1. Buckley, R. G., and Michaels, K. J.: Computed Tomography: A Powerful Tool in Solid Motor Exit Cone Evaluation. MDC H1457, March 1985.

2. Yeaple, F.: Cat Scan Becomes Engineering Test Tool. Design News, Vol. 62, April 1985.

3. Hendee, W. R.: The Physical Principles of Computed Tomography. Little, Brown and Co., 1983.

4. Newton, T. H.: Technical Aspects of Computed Tomography. G. D. Potts (editor), C. V. Mosby Co., 1981.

5. Schwartz, M. M.: Composite Materials Handbook. McGraw-Hill, Inc., 1984.

6. Barrett, J. E.: The Palapa-B2 and Westar-VI Missions: Final Report of the PAM-D STAR 48 Failure Investigation Committee, MDAC H1327, September 1984.

7. Static Test Report of TE-T-820-1, CCT-1, Contract NAS8-36303, prepared by Morton Thiokol, Inc., May 1985.

8. MSFC Hydrobuckle Investigation Report. In Publication, NASA TMX.

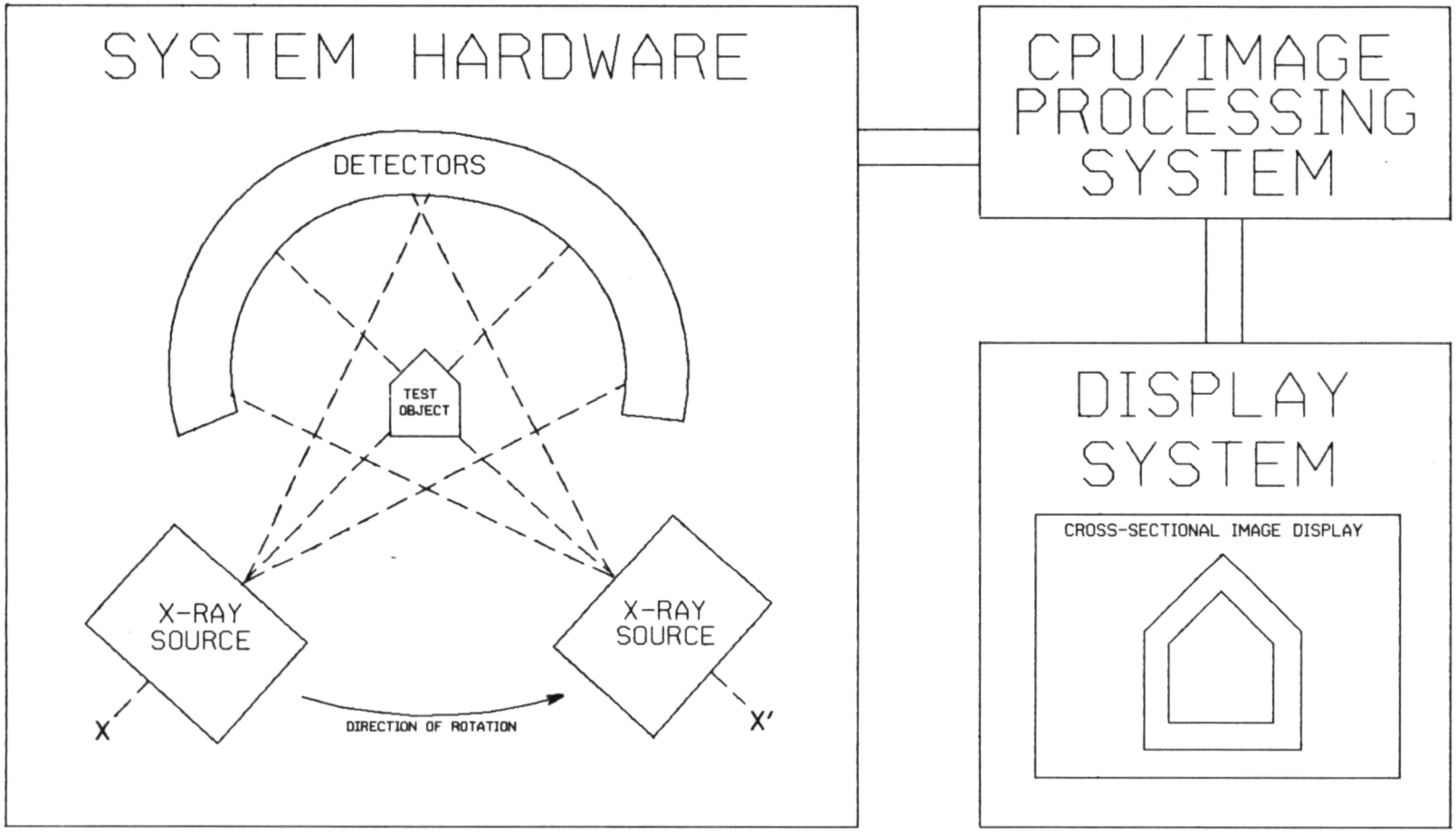

Figure 1. CT system components. Three components of every CT scanner. Note translation of source (X to X'). From 10 to 100 such translations may be required for a single reconstruction.

ORIGINAL PAGE IS
OF POOR QUALITY

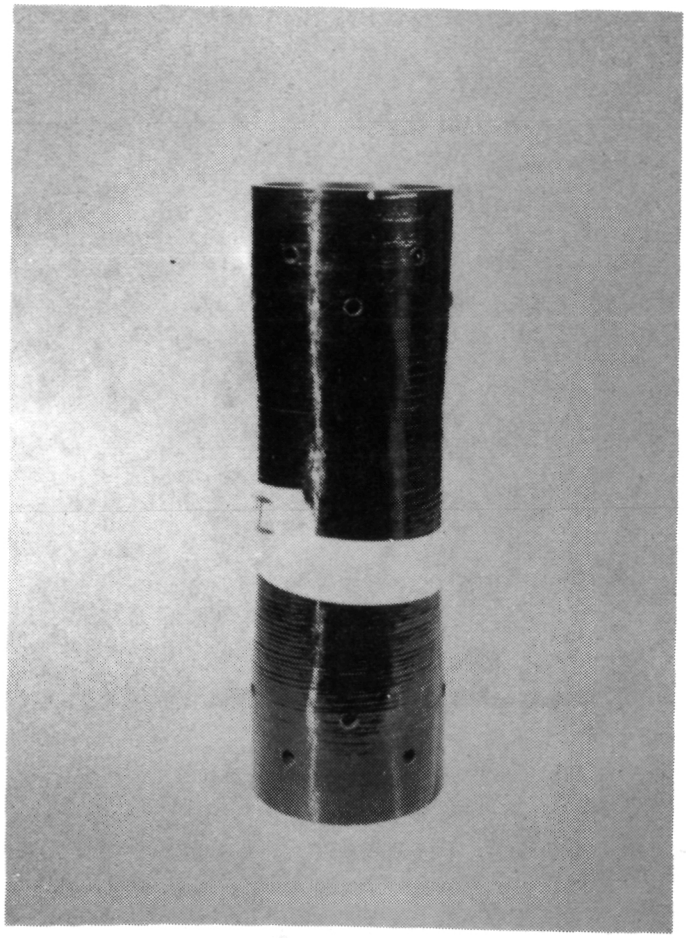

Figure 2. Graphite epoxy bipod strut. (Filament-bound strut measures 18 in. long by approximately 5.5 in. diameter. Visual taper is in OD only.)

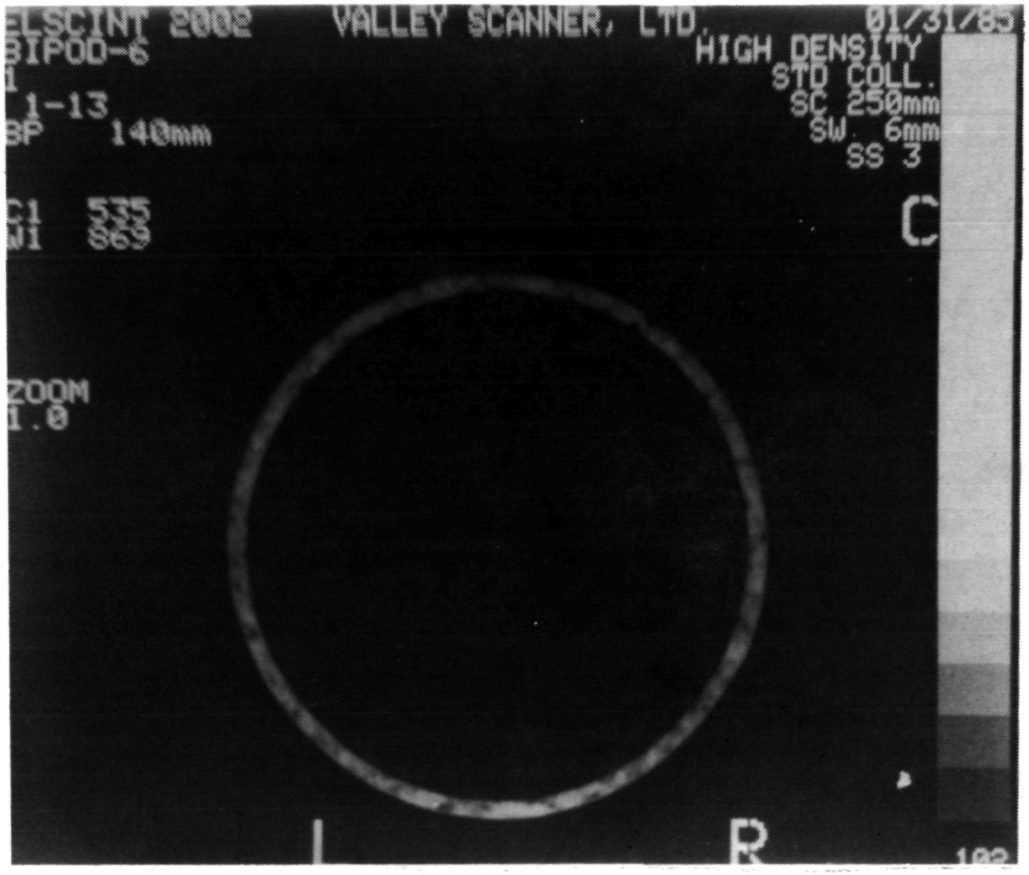

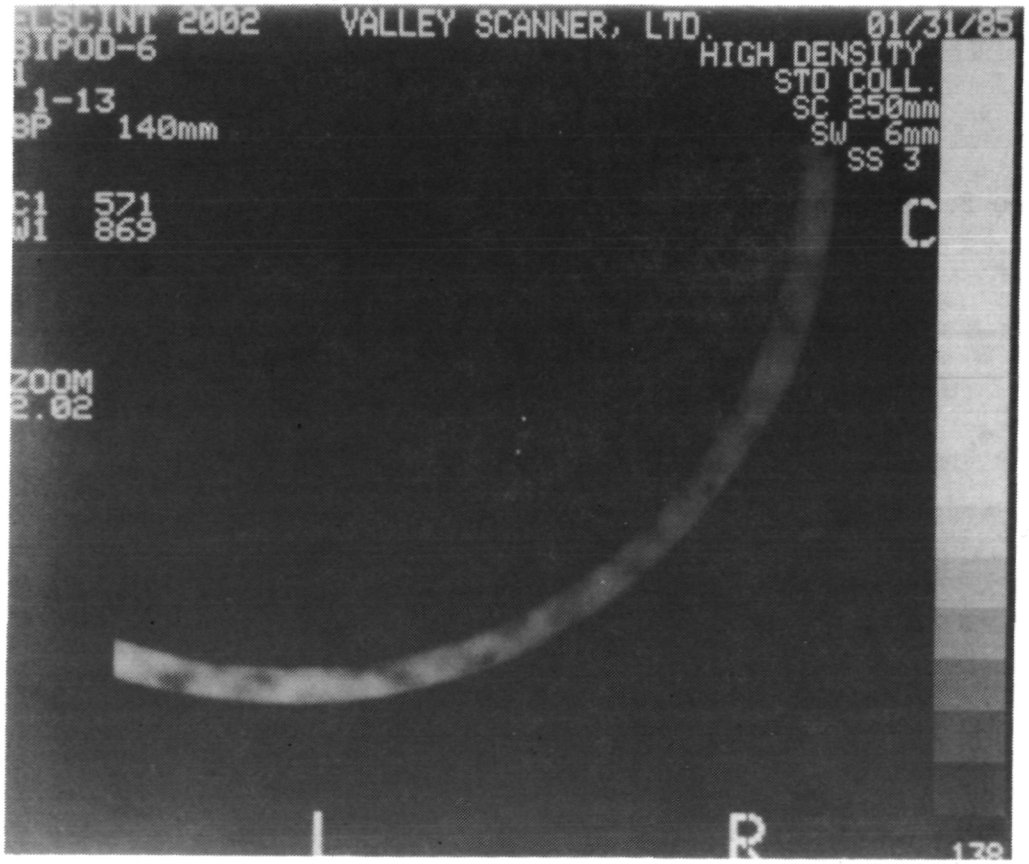

Figure 3. CT of GEBS. (a) Typical CT slice for GEBS. Note internal density variations. (b) Magnified view of three o'clock to six o'clock region from (a). Note void at four o'clock position.

ORIGINAL PAGE IS
OF POOR QUALITY

ORIGINAL PAGE IS
OF POOR QUALITY

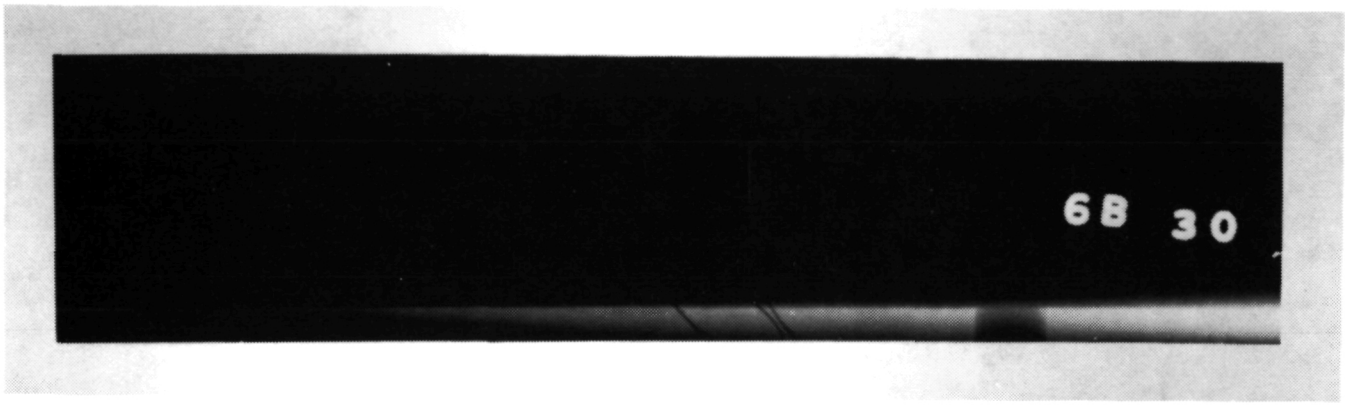

Figure 4. Tangential RT of GEBS. (Contrast and sensitivity of RT appears limited. Only indications noted are indistinct or artifactual.)

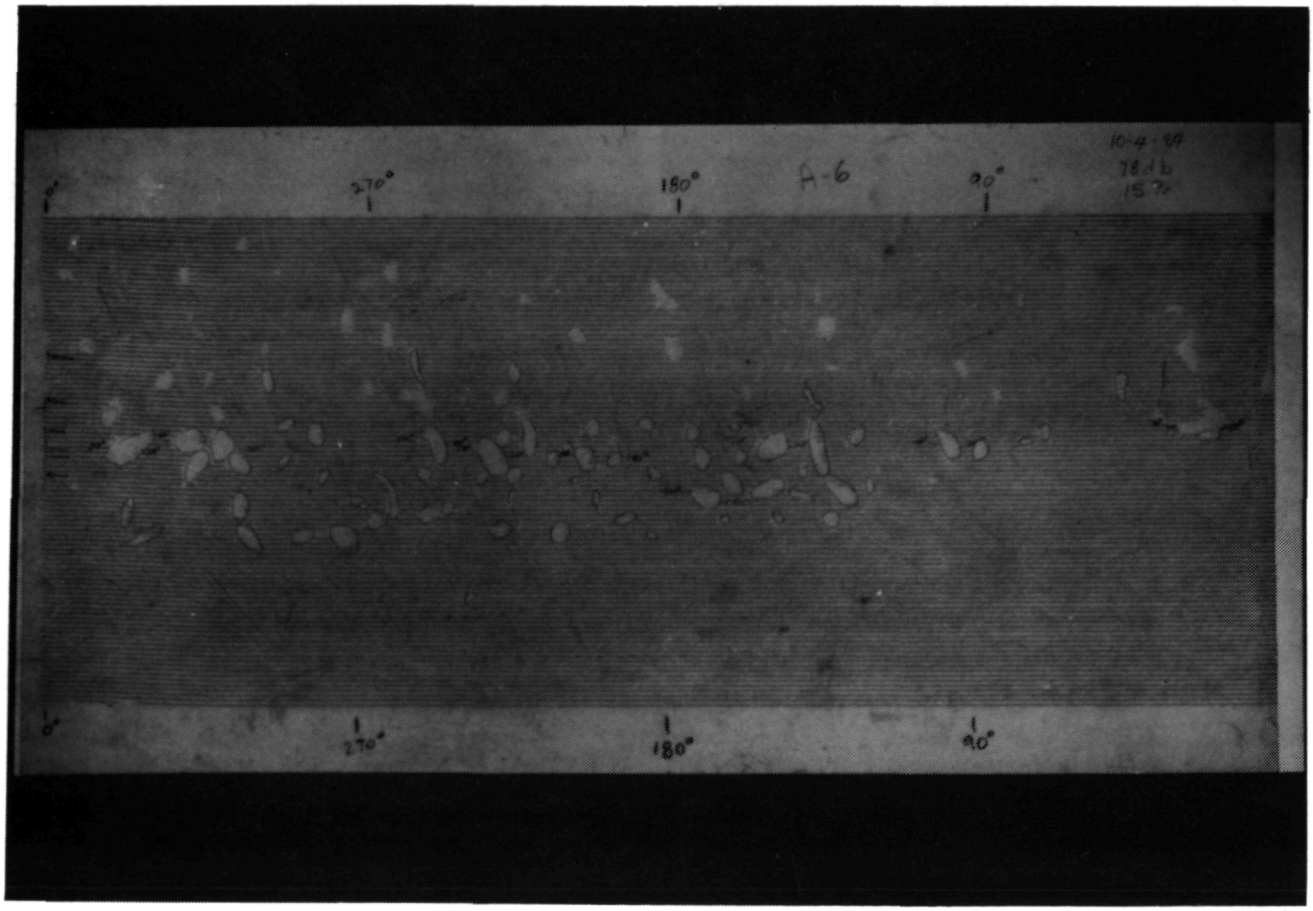

Figure 5. UT of GEBS. (Ultrasonic C-scan displays numerous delamination-like conditions in tapered wall region.)

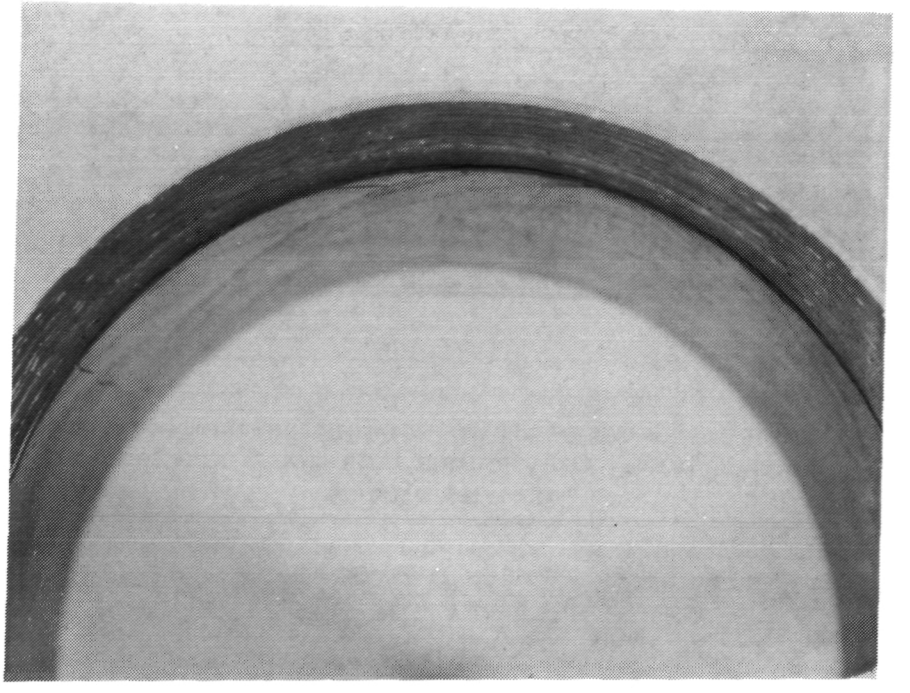

Figure 6. Delamination in GEBS. (Delamination visible through cylinder ID.)

ORIGINAL PAGE IS
OF POOR QUALITY

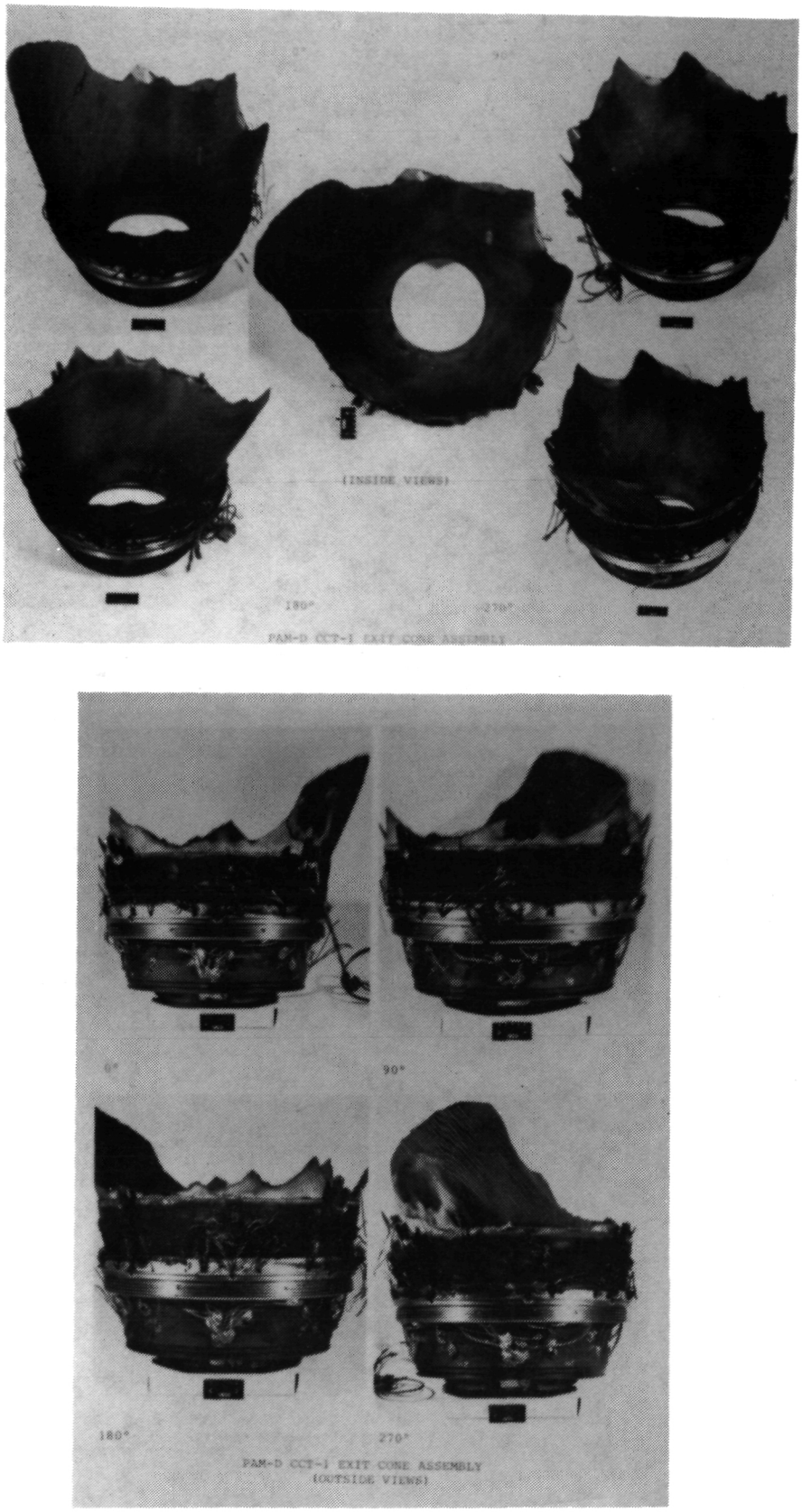

Figure 7. CCT-1 exit cone assembly. (a) Interior of carbon-carbon exit cone. Truncated cone due to sea-level induced buckling aft of insulator.

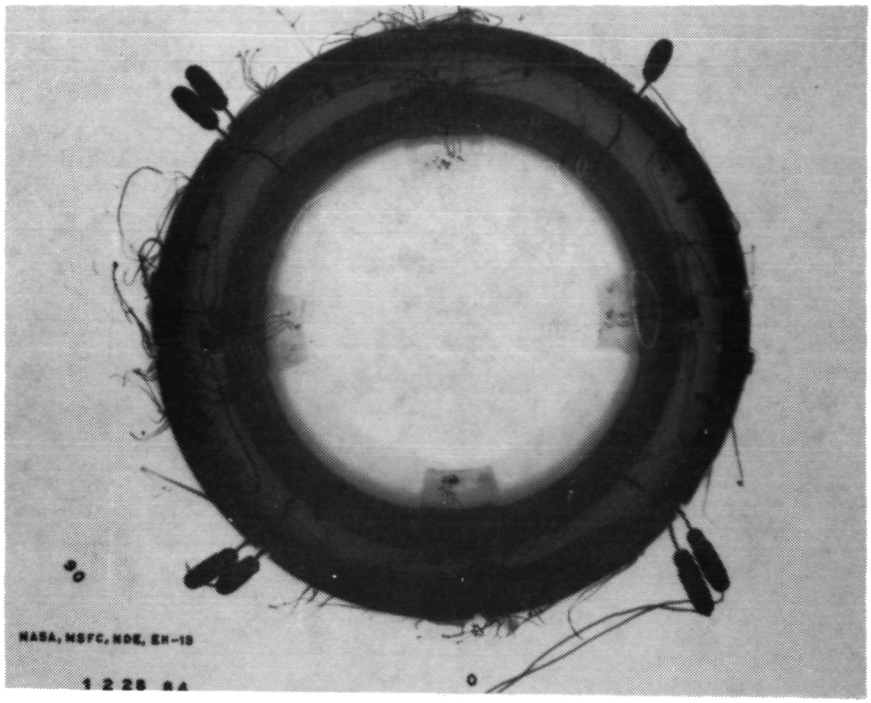

Figure 8. Axial RT of CCT-1. (While resolution in x-ray print is inferior to characterized film, several indications are visible, including instrumentation, flow patterns, and bond gap.)

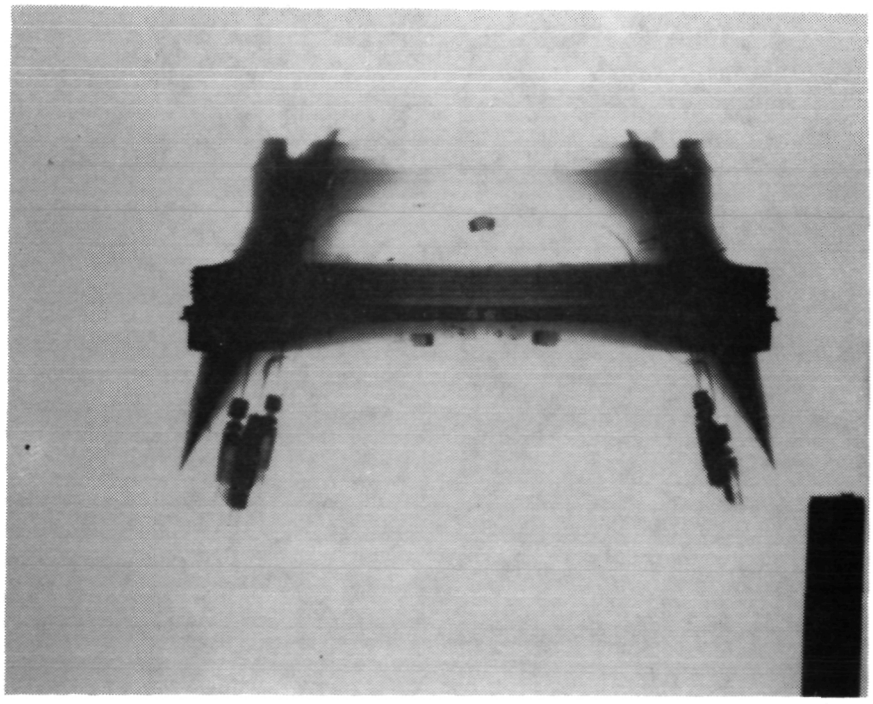

Figure 9. Tangential RT of CCT-1/MTI/E. (Pressure transducers, instrumentation, and o-ring bond gap, while visible, lack clarity. View is 180 deg true tangential.)

ORIGINAL PAGE IS
OF POOR QUALITY

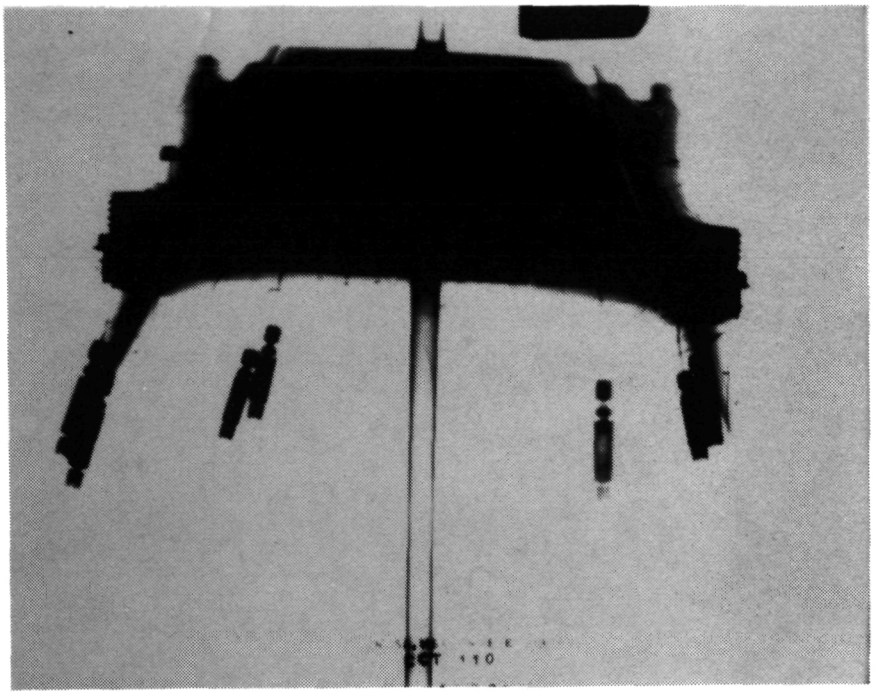

Figure 10. Tangential RT of CCT-1/MSFC. (Post-test RT of CCT-1 supported by CT alignment fixture. Note circumferentially non-uniform gap. View is 110 deg true tangential.)

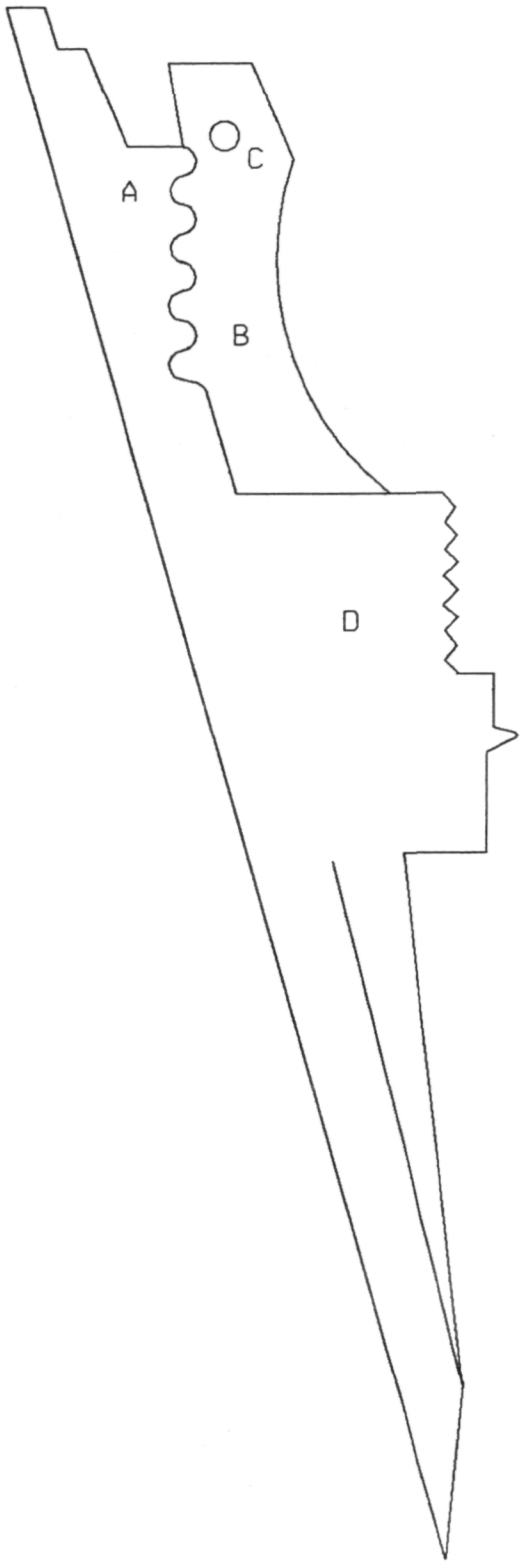

Figure 11. Tangential RT map. [Location guide for CCT-1 correlation effort (A = carbon-carbon exit cone, B = carbon-phenolic, C = o-ring, D = titanium ring).]

ORIGINAL PAGE IS
OF POOR QUALITY

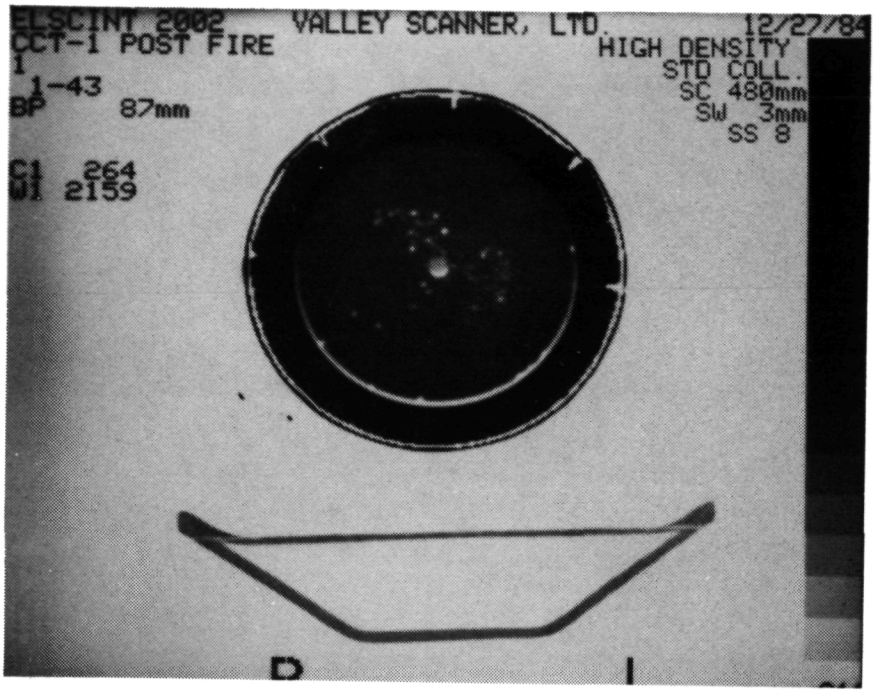

Figure 12. CCT-1 CT scan anomalies. (Strobing effects from pins and titanium adaptor are evident. High-density indications in interior are due to alignment fixture artifacts.)

(a)

(b)

Figure 13. CCT-1 CT scan/bond gap. (Circumferentially non-uniform bond gap is evident in this thread region slice. Note flow region at 20 deg position.) (a) at 33 mm. (b) At 36 mm.

ORIGINAL PAGE IS
OF POOR QUALITY

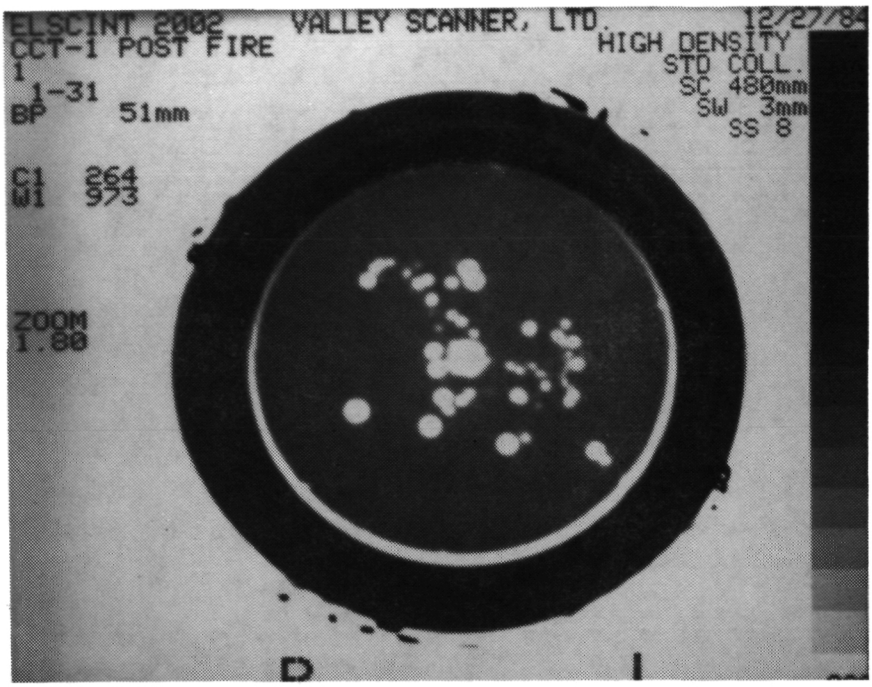

(a)

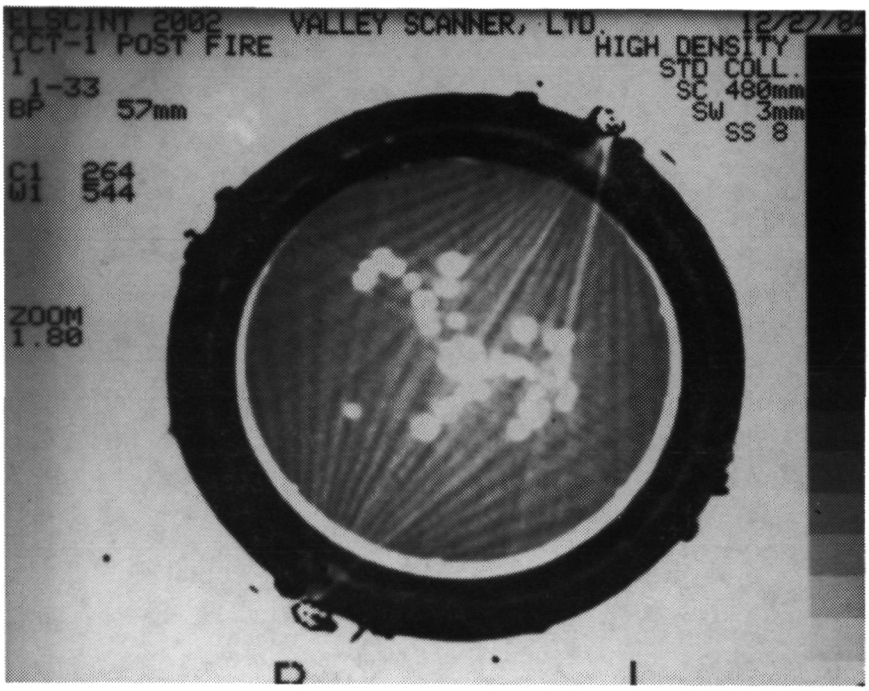

(b)

Figure 14. CCT-1 CT scan/bond gap. (a) While not as evident as in forward thread regions, bond gap non-uniformity is still present. (b) Strobing and high-density inclusions in the bond gap.

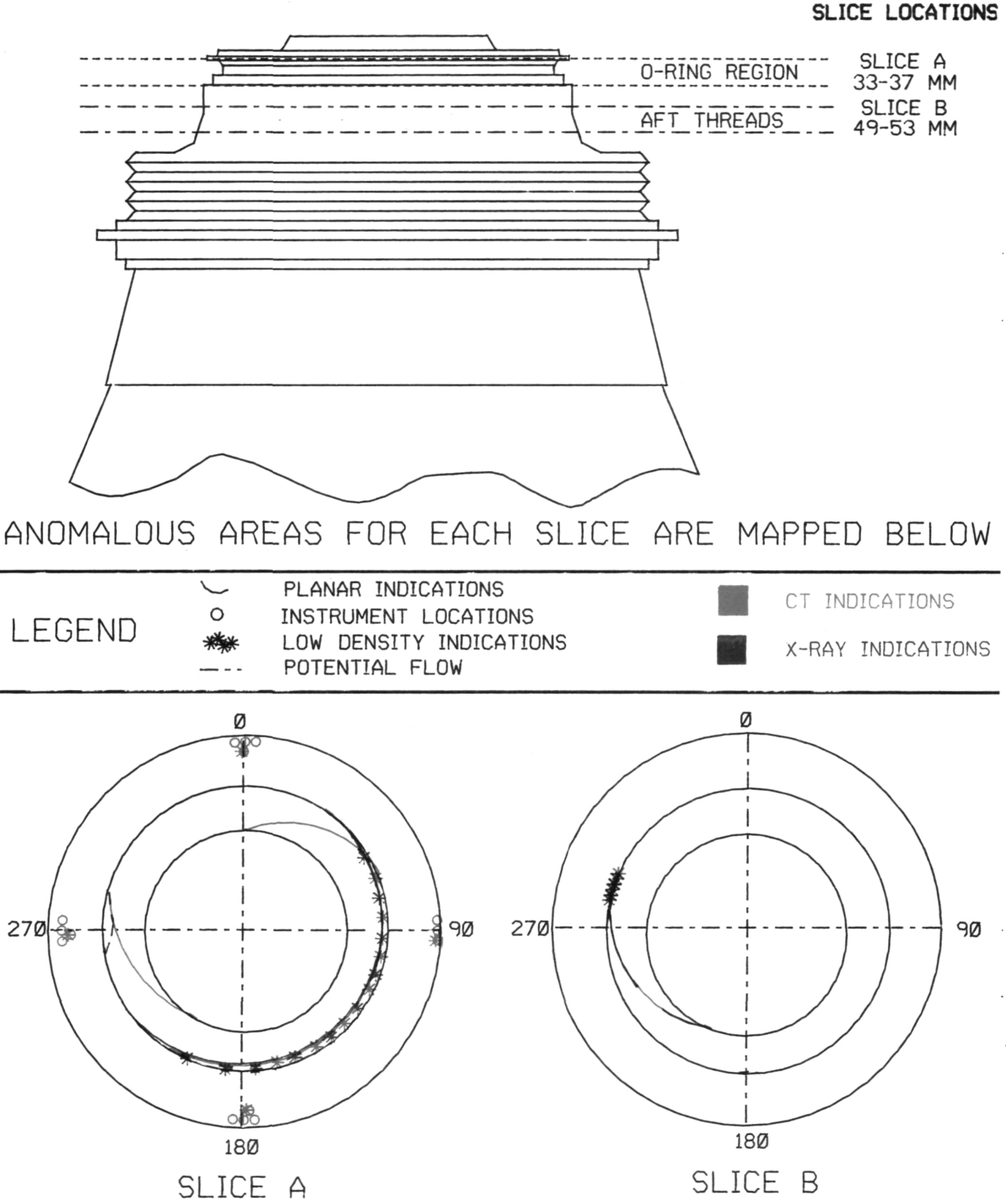

Figure 15. CCT-1 data correlation map. (The correlation for the anomaly types is clearly indicated.)

ORIGINAL PAGE IS
OF POOR QUALITY

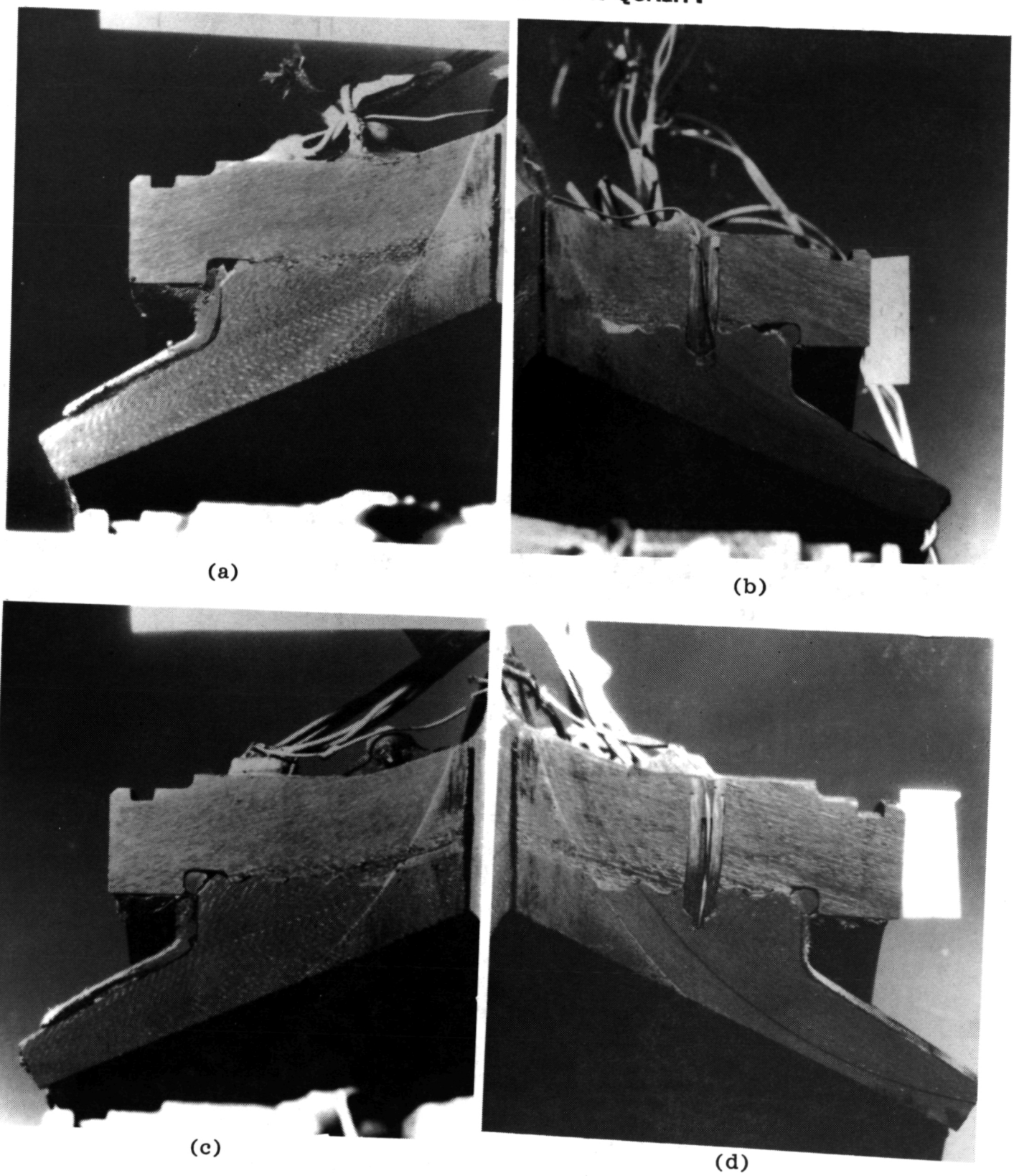

Figure 16. Cross-section of CCT-1/forward segment. (Visual observations reveal circumferentially non-uniform O-ring gap, varying amounts of adhesive in the thread region, and a slight axial shifting of the exit cone.)

ORIGINAL PAGE IS
OF POOR QUALITY

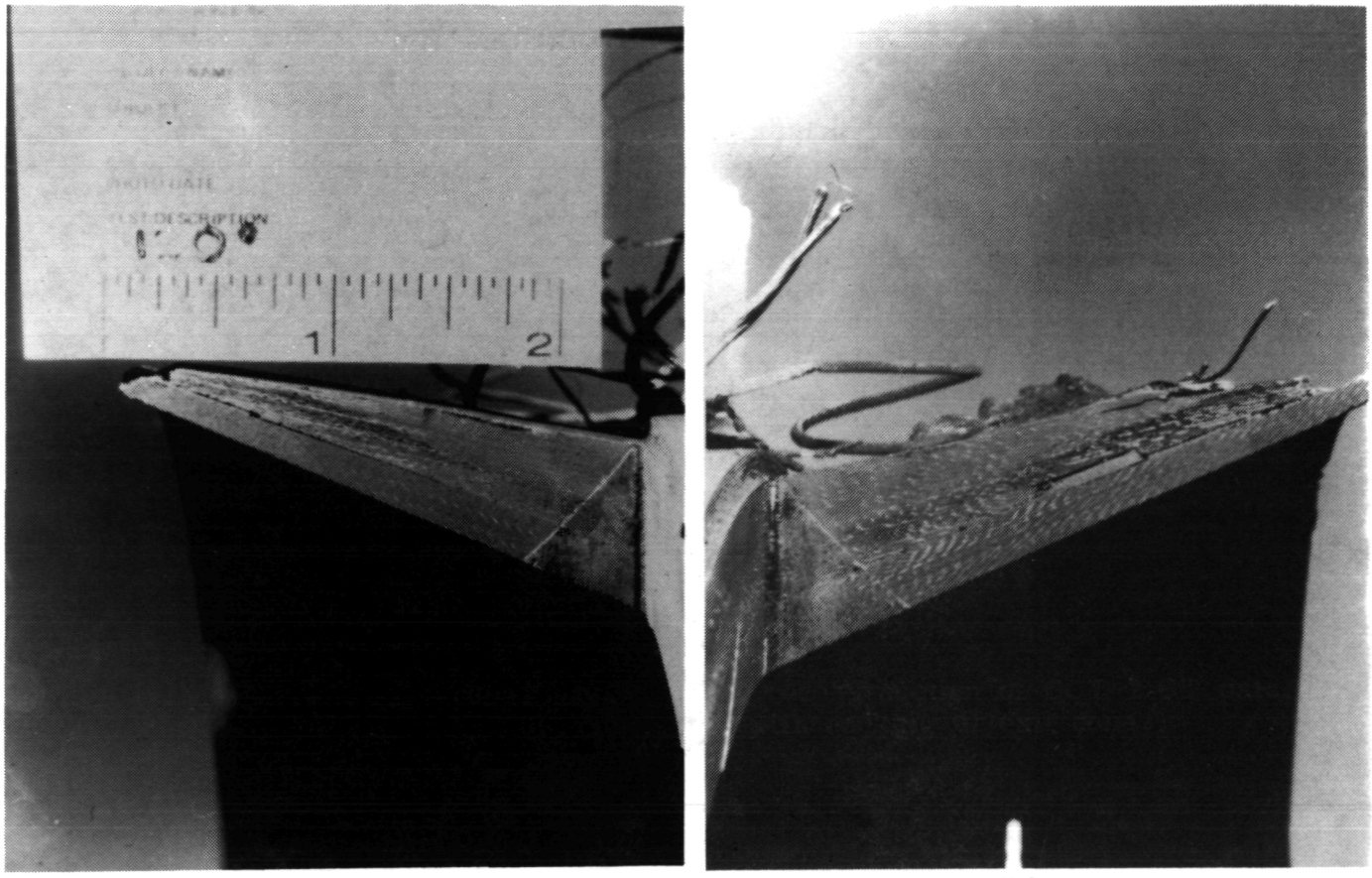

(a) (b)

Figure 17. Cross-section of CCT-1/aft segment. (Visual observations reveal instrumentation sites, delamination region (b), and char indications.)

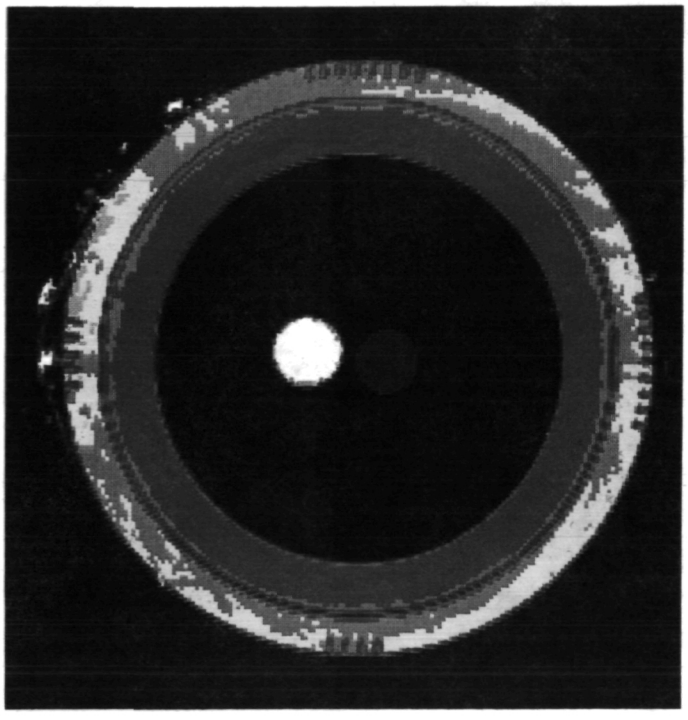

Figure 18. CCT-2 CT/preliminary. (MSFC reconstruction of CCT-2 CT data. Note non-uniform bond, consistent with cocking of exit cone.)

ORIGINAL PAGE IS
OF POOR QUALITY

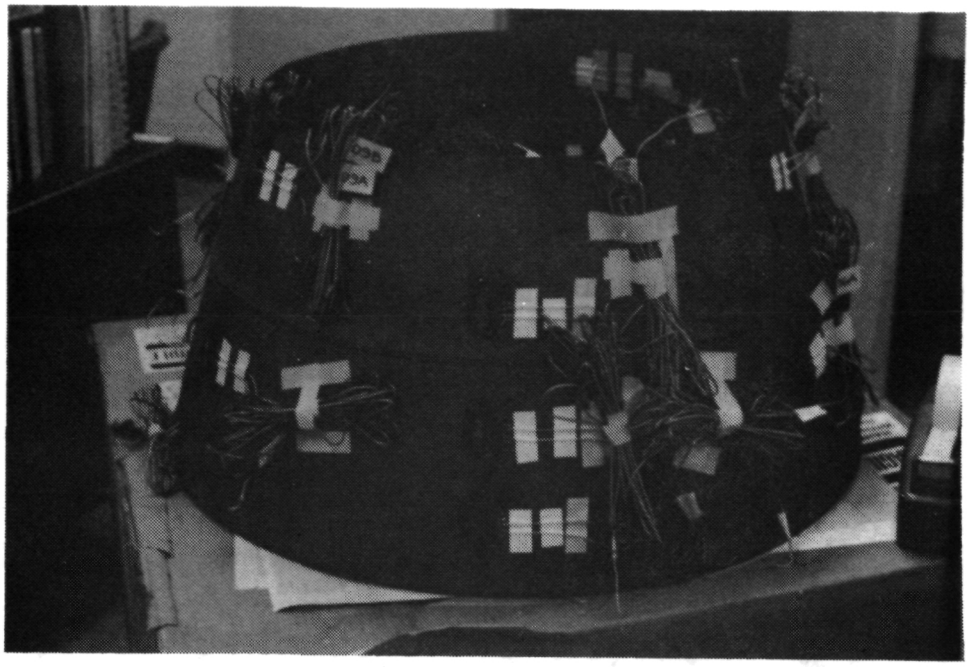

Figure 19. Instrumented cone. (Aft section from CCT-1 instrumented for hydrobuckle test.)

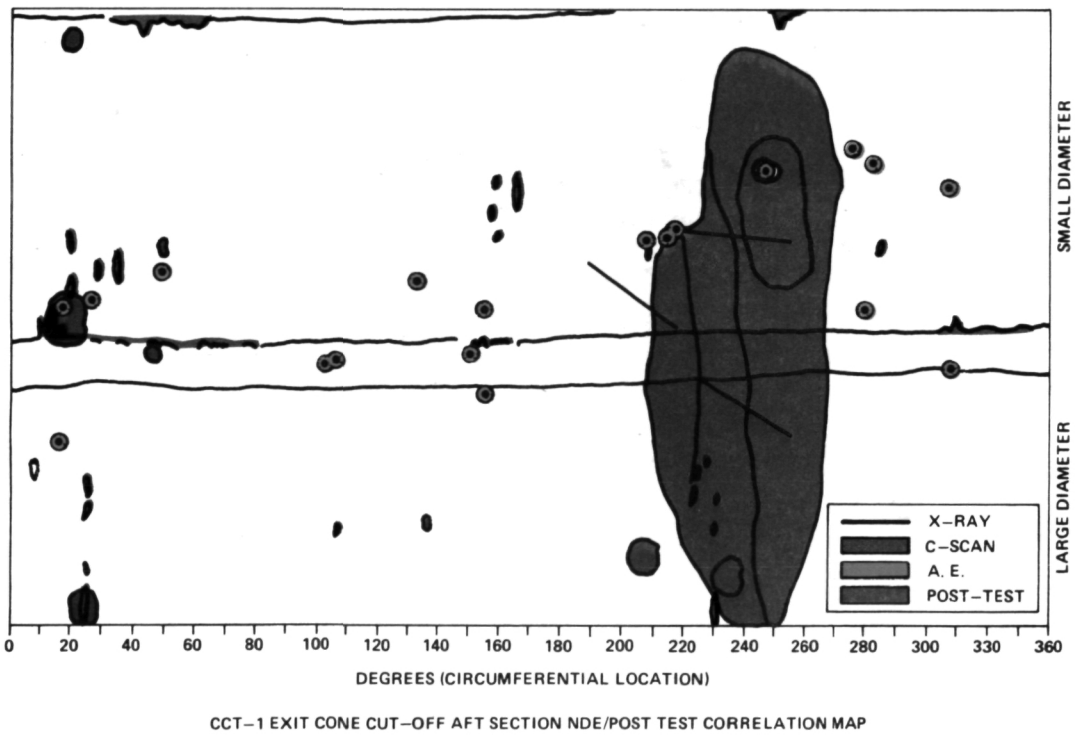

Figure 20. NDE correlation map/hydrobuckle test. (Green indications - UT scan regions of high attenuation; straight black lines located at 200 deg and 260 deg x-ray planar indications; two black dots at 210 deg and 240 deg - high-density inclusion/missing fiber region/ red circles - acoustic emission data; blue regions - post-test observations.)

Figure 21. Post-test cone. (Buckled region of test cone. Note surface crazing in region left of buckle center-line below stiffener ring.)

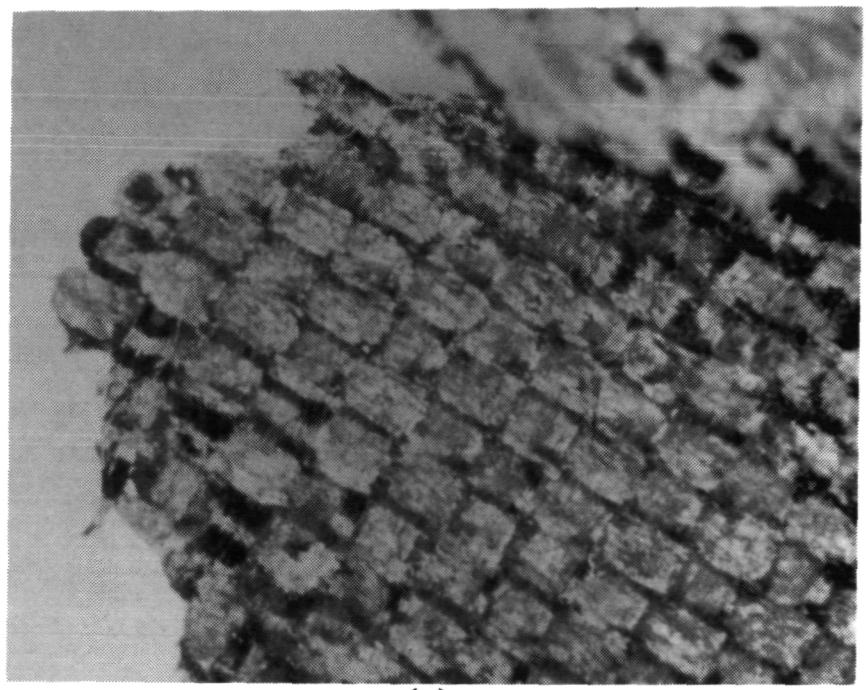

(a)

Figure 22. 220 deg region micrographs. (a) Crack juncture outside of matrix-full region; fiber bundle surfaces not evident. (b) Crack juncture inside; rougher surface appearance, some fiber bundle surface visible. (c) Dry ply region below stiffener ring crackes surface; high incidence of visible matrix-poor clean fiber bundles.)

ORIGINAL PAGE IS
OF POOR QUALITY

(b)

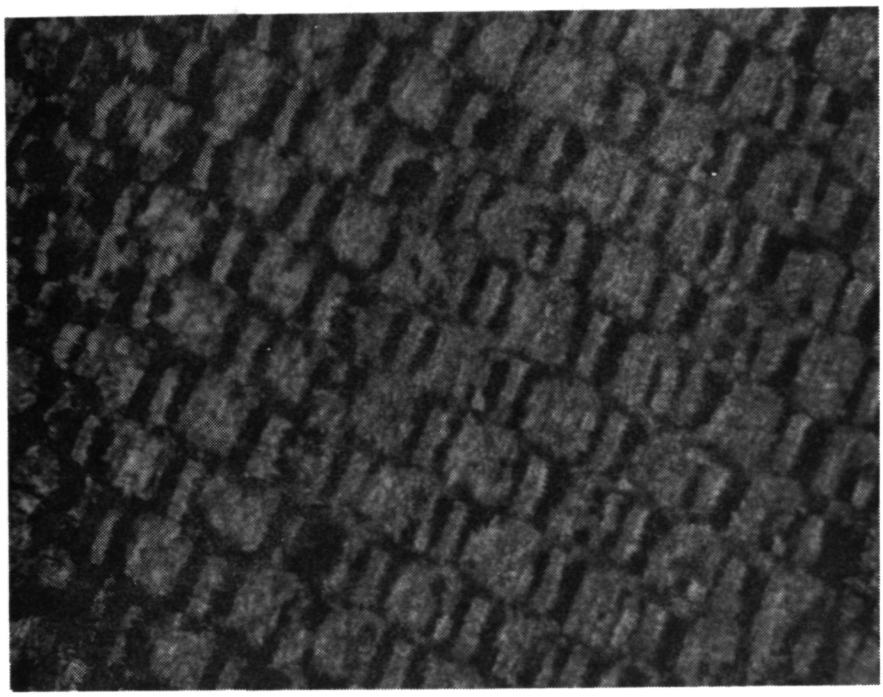

(c)

Figure 22. (Concluded).

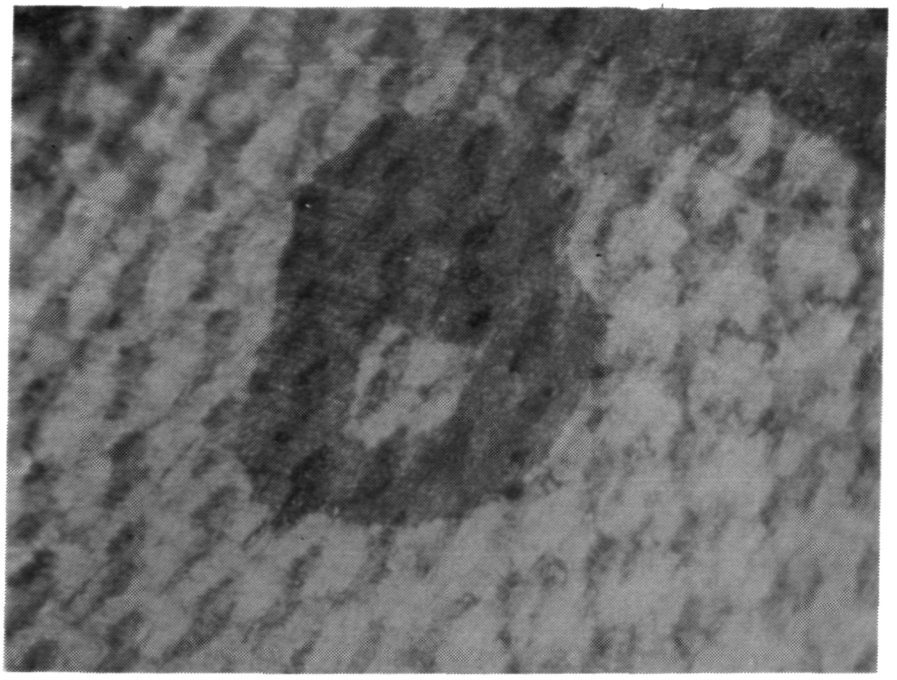

Figure 23. 240 deg surface indication. (Surface indication is clearly shallow and does not appear to affect internal fibers.)

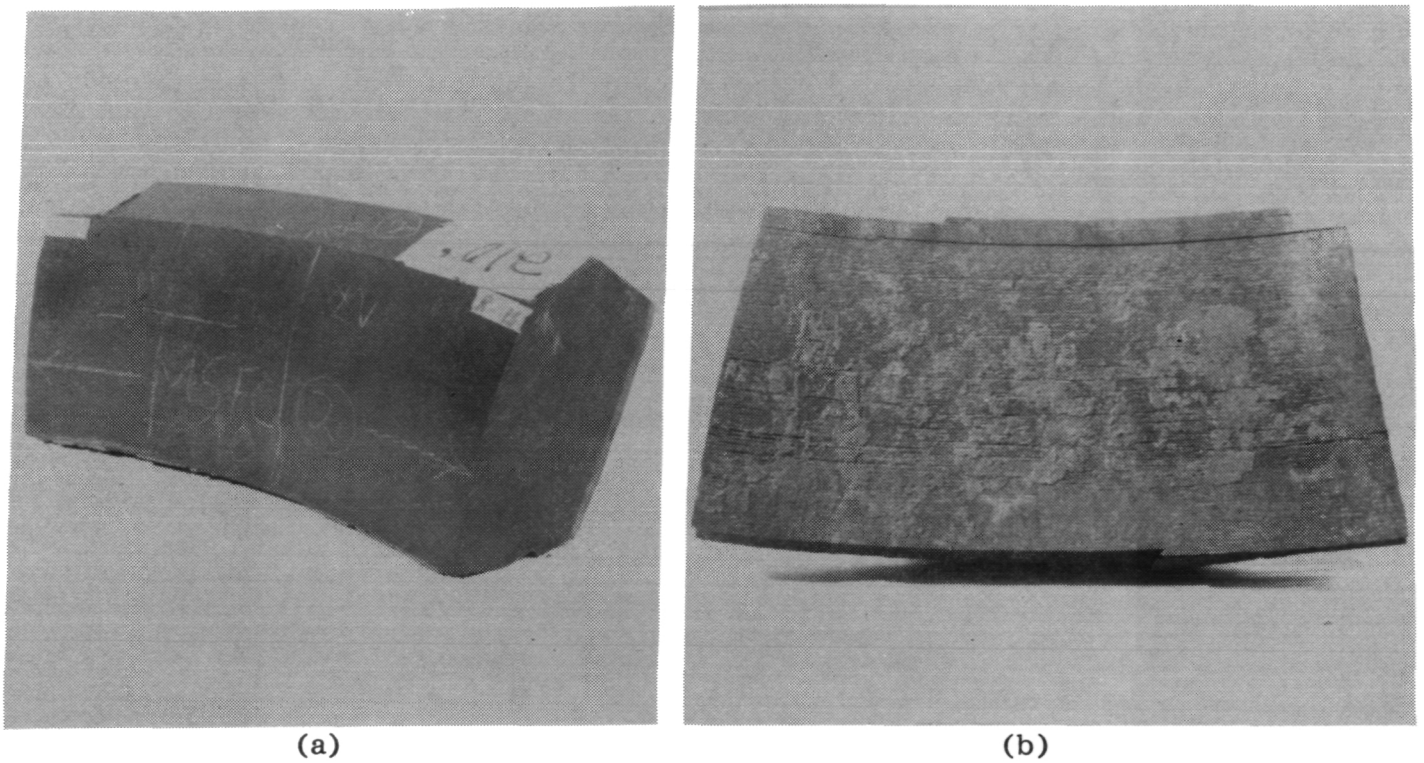

(a) (b)

Figure 24. Representative SRM segment samples. (a) Unfired segment marked for test. Light region on OD is composed of silica phenolic. (b) Fired SRM segment. Note char and delamination regions.

ORIGINAL PAGE IS
OF POOR QUALITY

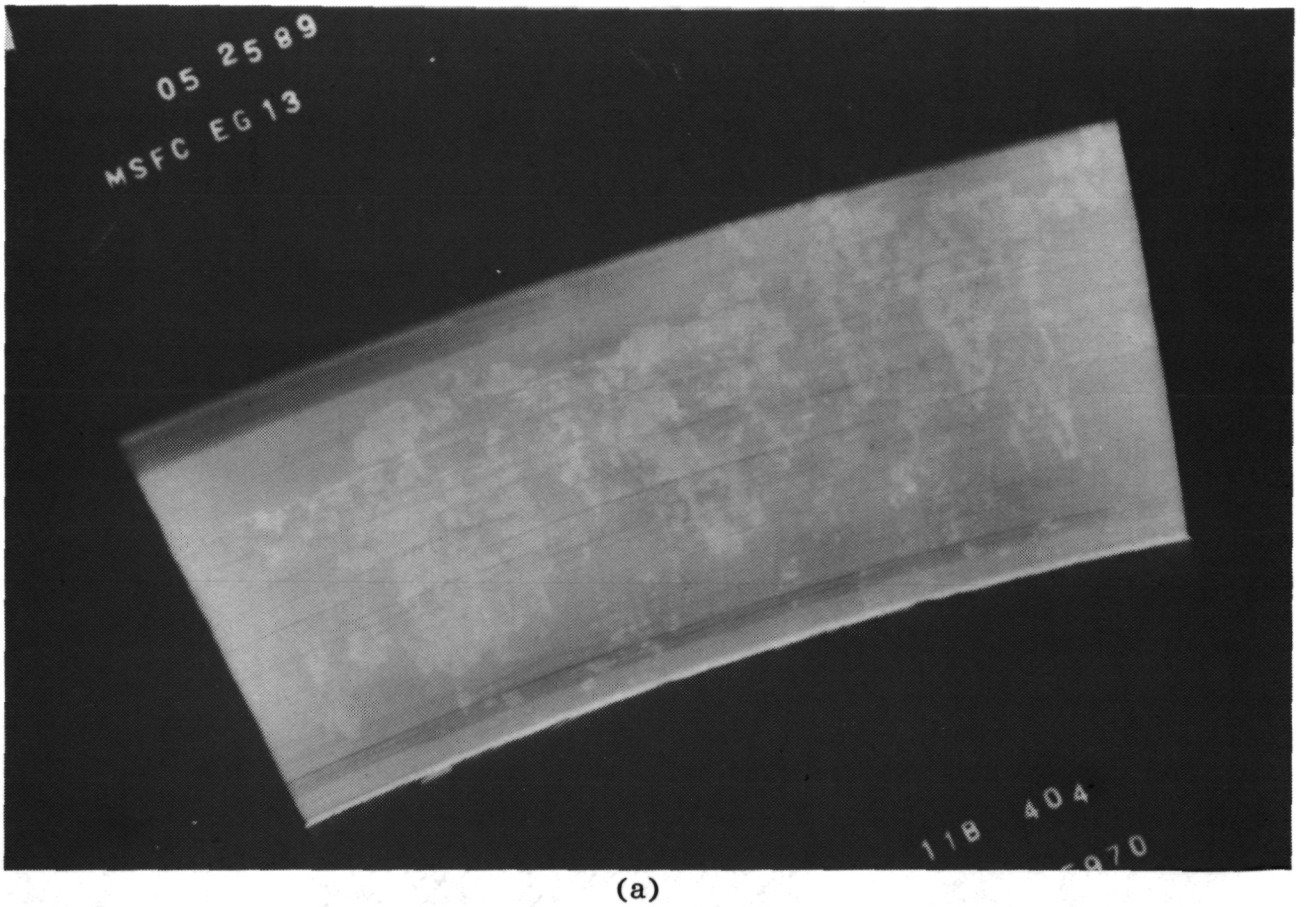

(a)

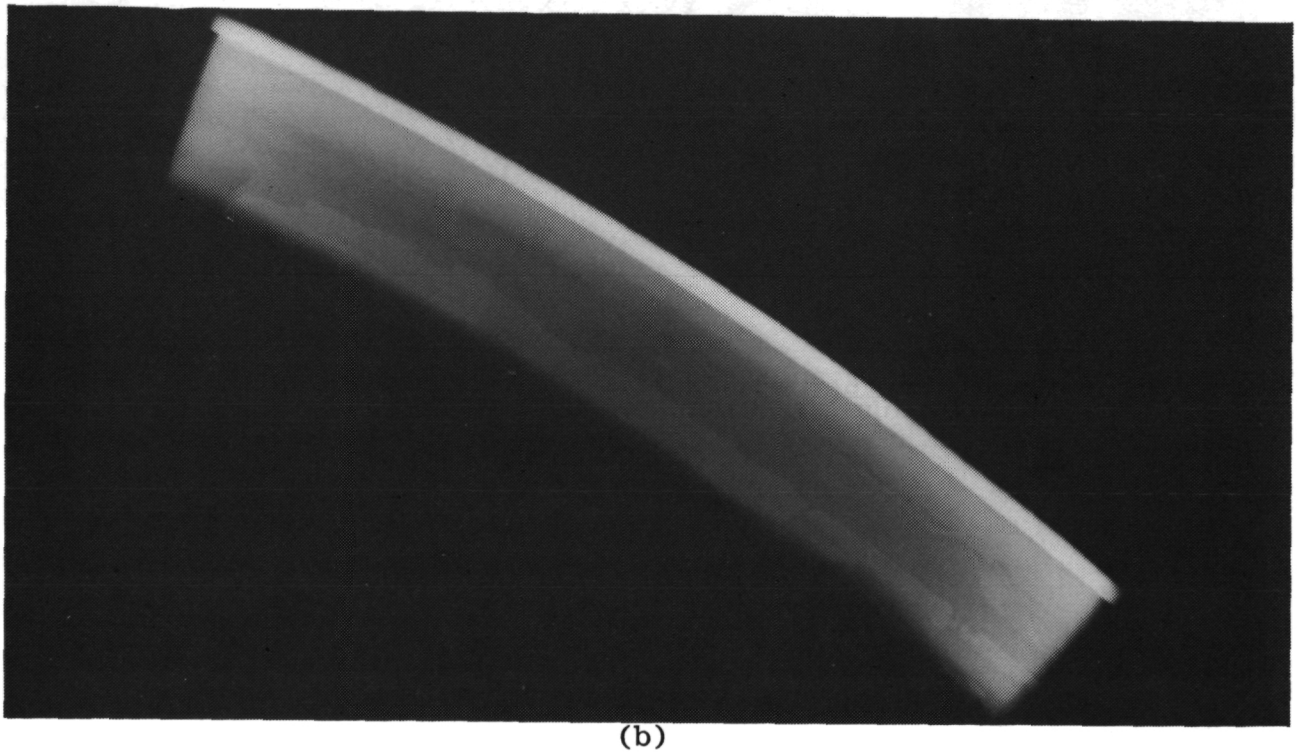

(b)

Figure 25. Radiography of fired SRM samples. (a) Radial view. Note char and erosion pockets, delaminations, and cloth patterns. (b) Tangential view. Dark, low-density region on ID reflects char zone. Variable density indications through segment are artifacts due to rubber insulator material on base. (See Figure 24.)

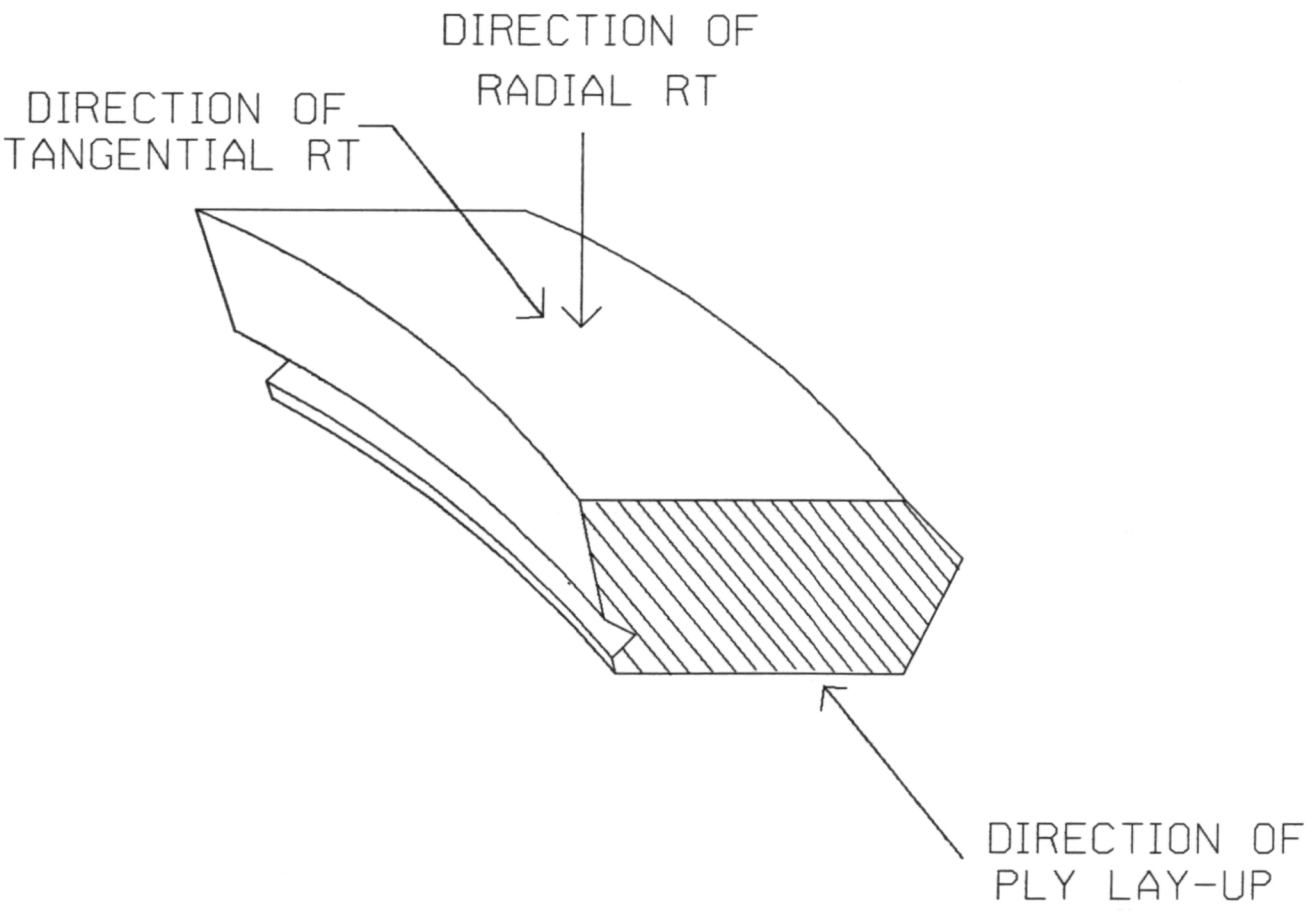

Figure 26. SRM radiographic planes. (To eliminate superpositioning between plys, true tangential RT was applied.)

ORIGINAL PAGE IS
OF POOR QUALITY

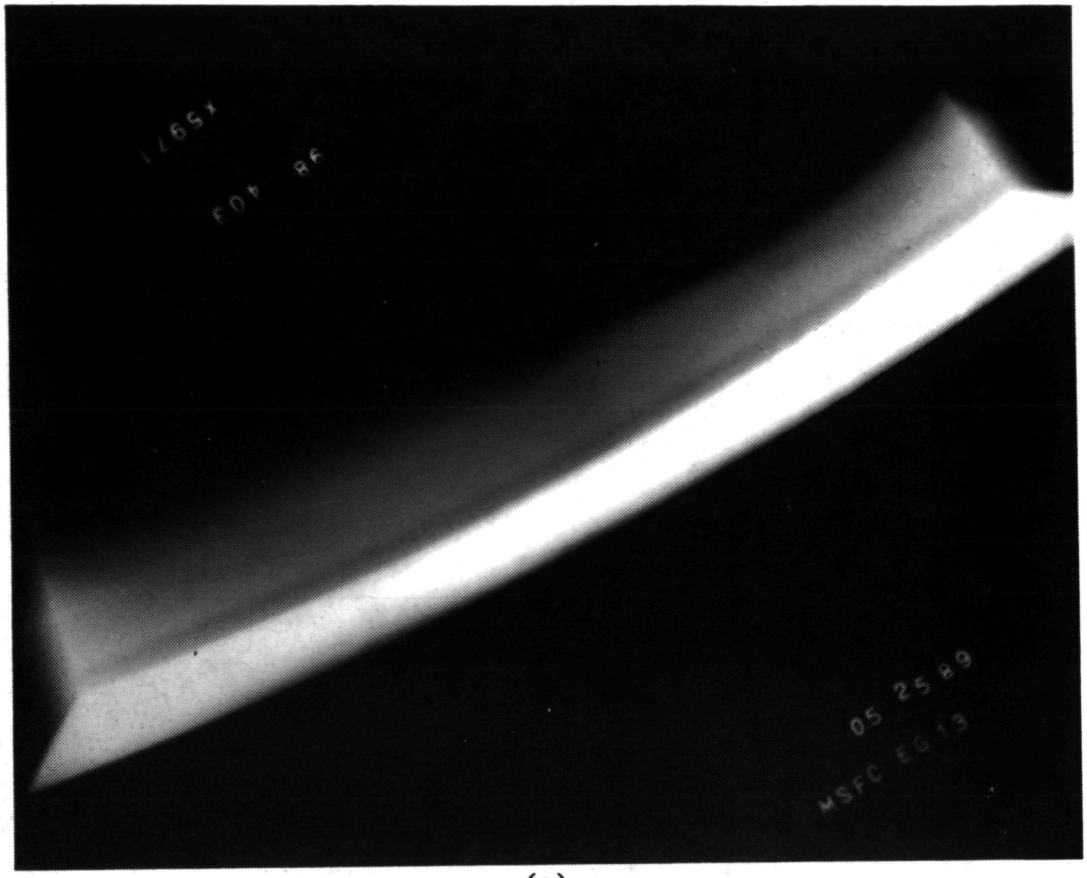

(a)

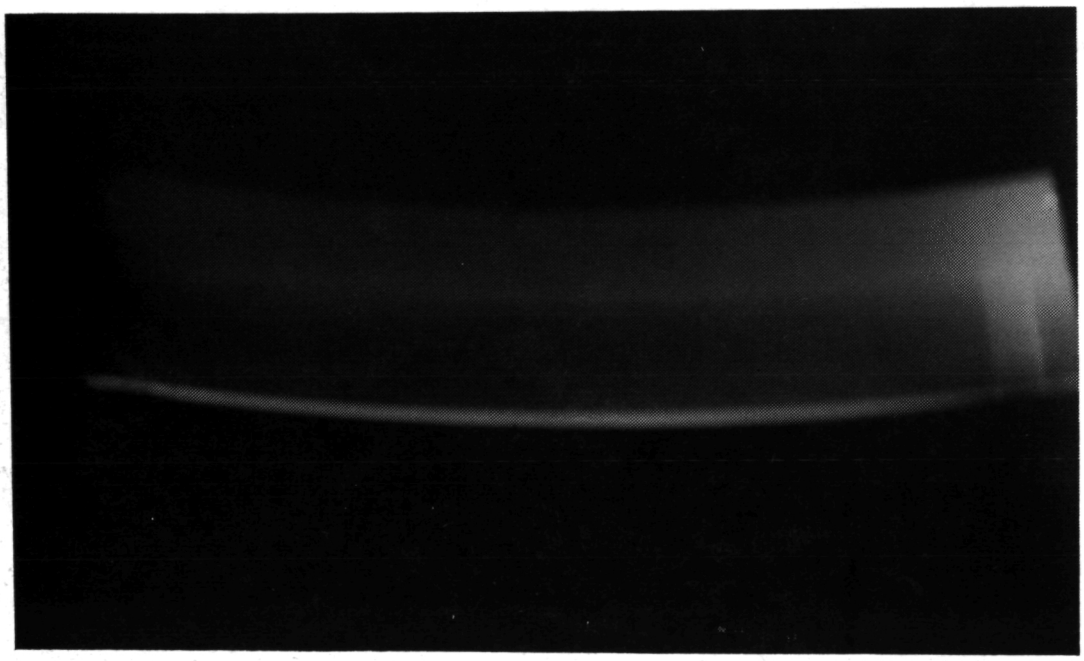

(b)

Figure 27. RT of unfired SRM sample/true tangential. (a) initial tangential view reflects ply superpositioning effects through anomalous density variability and diminished resolution. (b) True tangential view shows improved contrast and reduction of ply superpositioning effects.

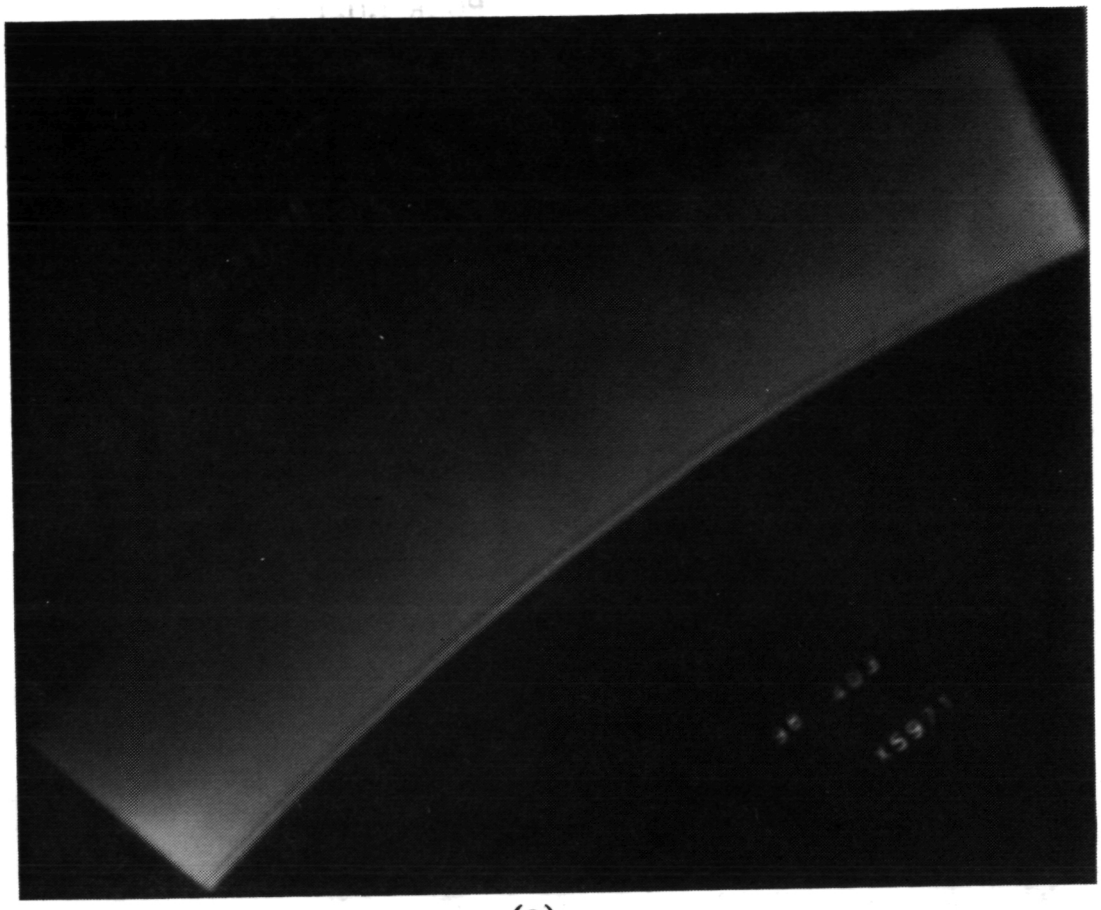

(a)

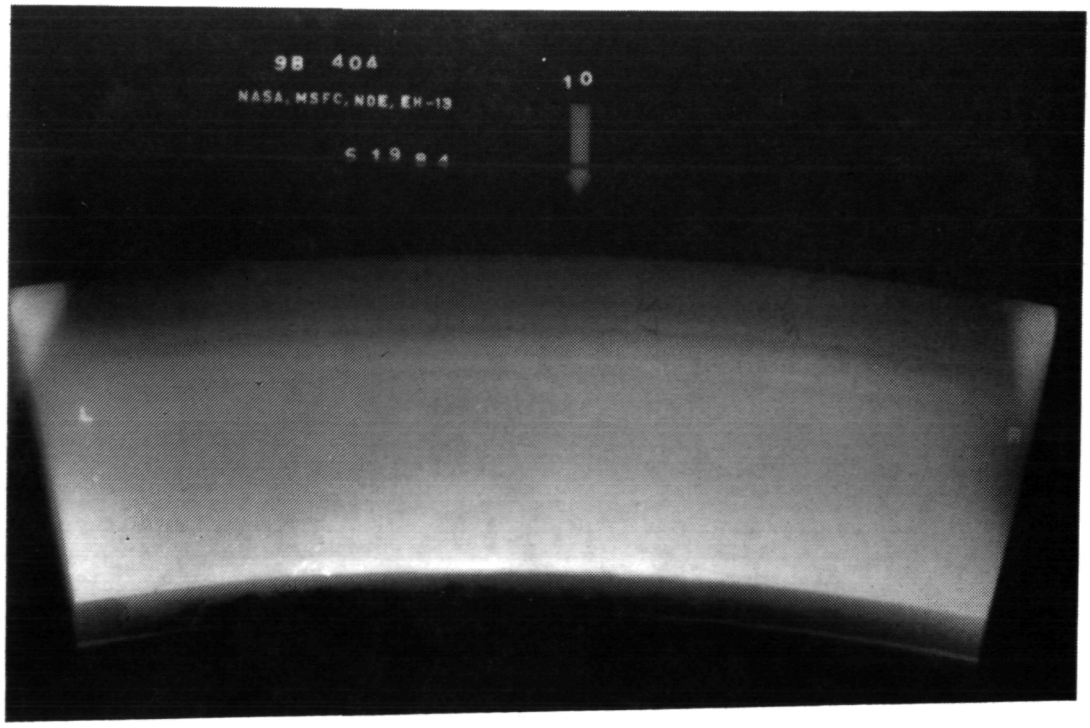

(b)

Figure 28. RT of unfired SRM samples/radial. (a) Note internal density variations, cloth patterns, and cloth-to-cloth lacing patterns. (b) Note delaminations, resin-starved regions, and cloth patterns.

ORIGINAL PAGE IS
OF POOR QUALITY

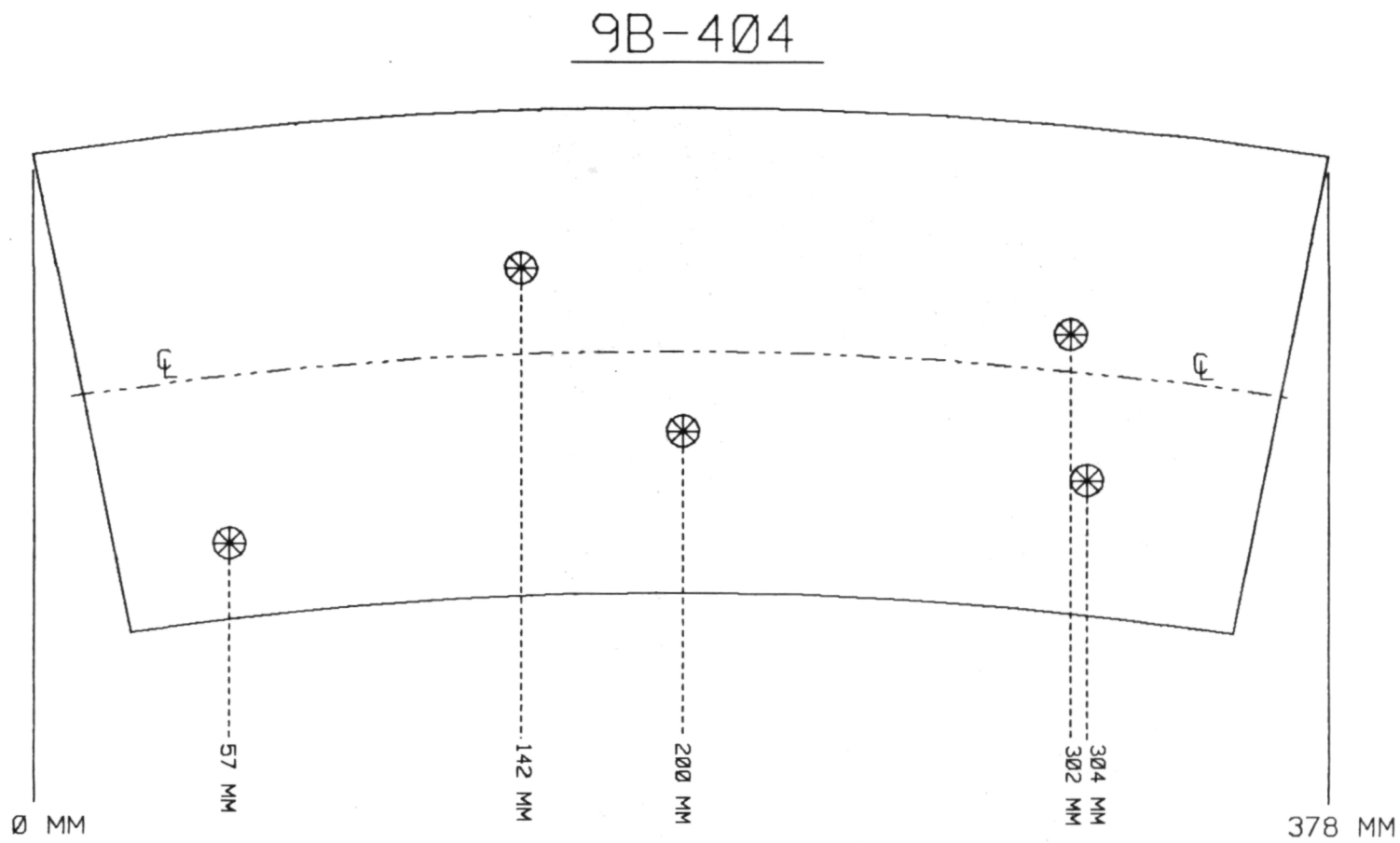

COMMENTS: ⊛ DENOTES ANOMALY TO BE FURTHER INVESTIGATED
ALL DIMENSIONS GIVEN IN MM
DIMENSIONS SHOWN ARE OF PROJECTED SIZE

Figure 29. SRM surview sketch. (Location guide for CT of SRM samples.)

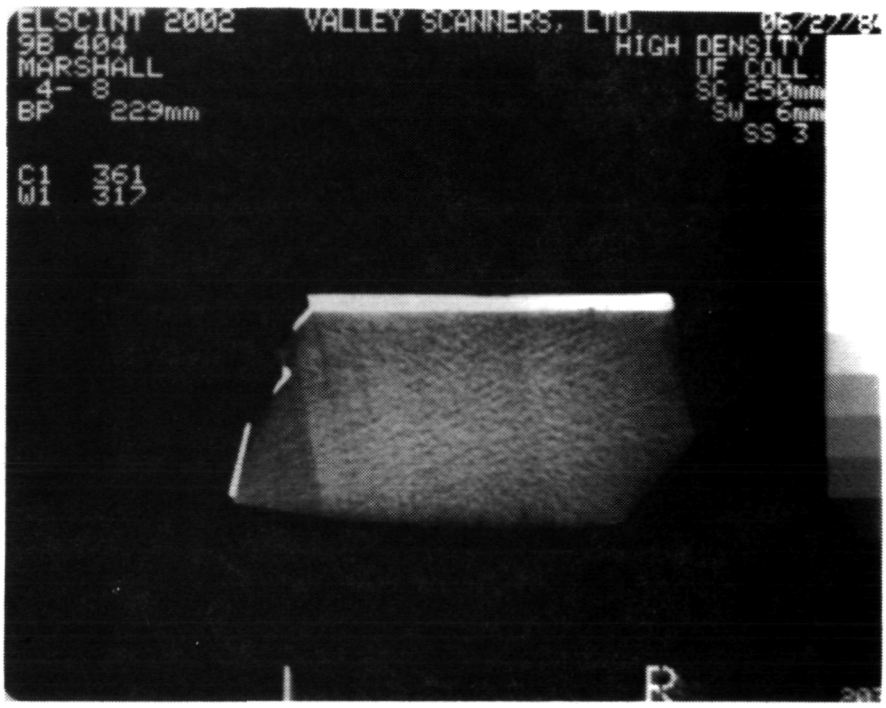

Figure 30. CT of unfired SRM sample/tangential. (Dark band on left side of image may result from cure cycle variations. Delaminations and resin-starved regions also appear.)

ORIGINAL PAGE IS
OF POOR QUALITY

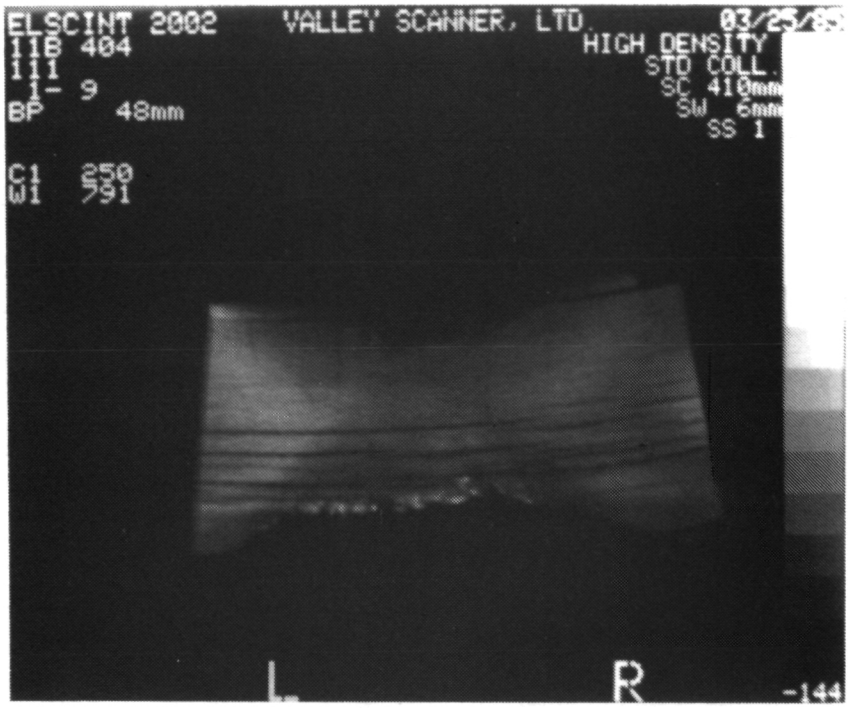

(a)

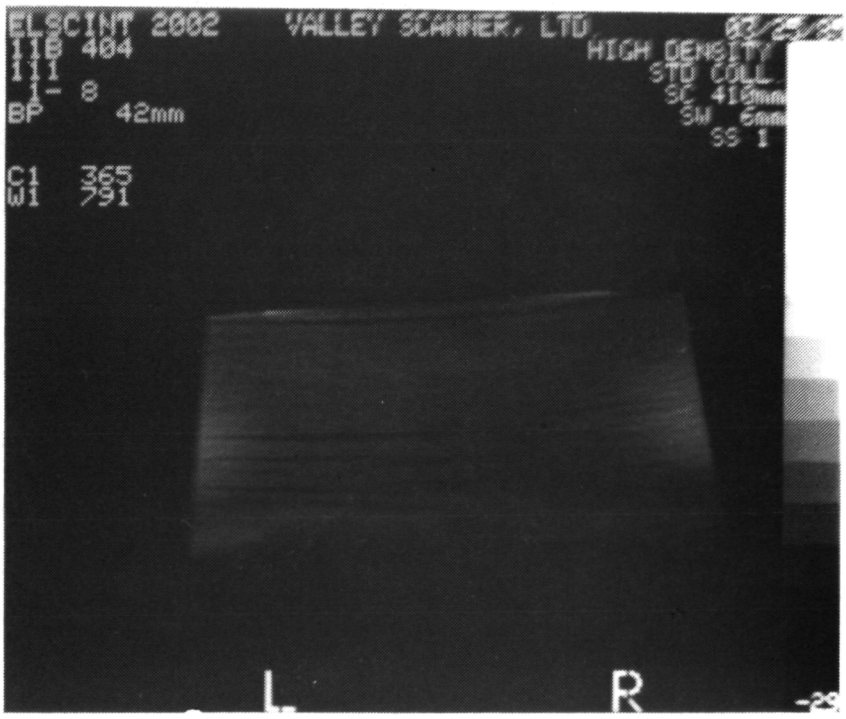

(b)

Figure 31. CT of fired SRM sample/axial. (a) Char/erosion patterns and delaminations are visible in the segment. (b) Further into the sample, delaminations still appear. Char/erosion patterns are less apparent.

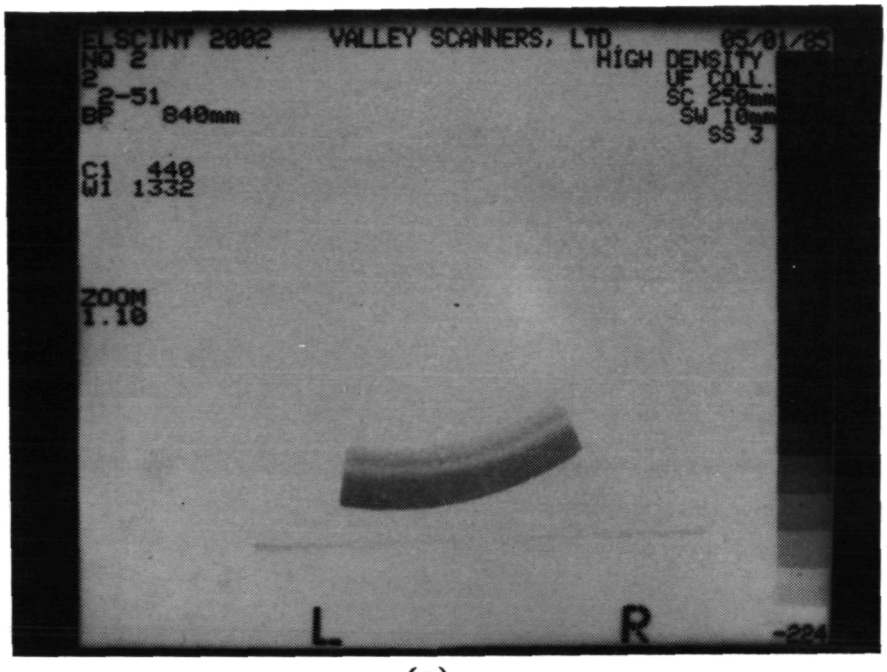

(a)

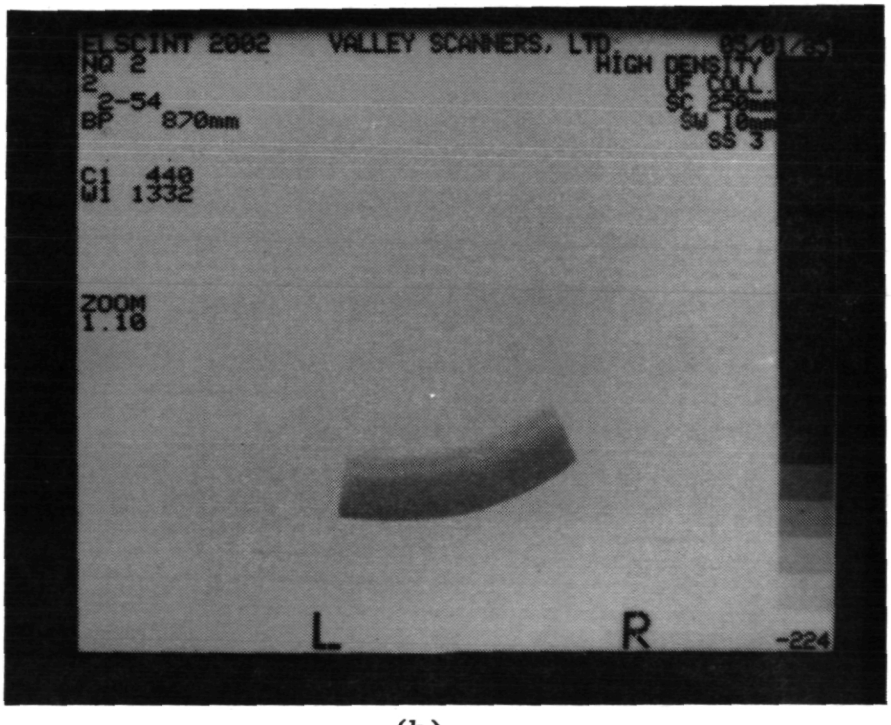

(b)

Figure 32. CT of NQ2/forward section. (a) Char/heat-affected regions are delineated by minimum density regions. (b) Identical to (a). Note clarity of char profile.

ORIGINAL PAGE IS
OF POOR QUALITY

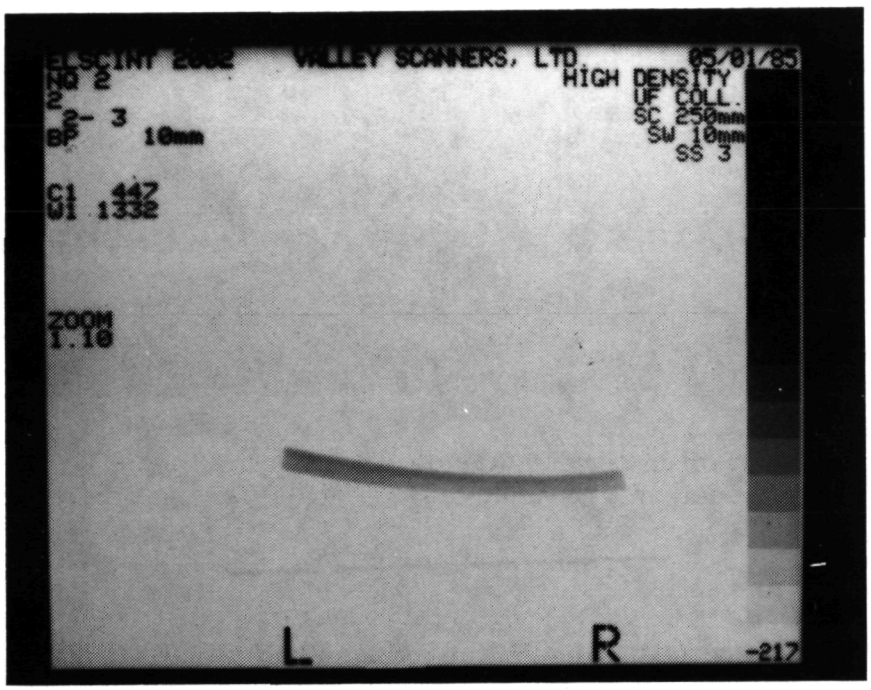

Figure 33. CT of NQ2/aft section. Char profile remains visible. Mapping subjectivity, even in thin regions, is clearly reduced.

TABLE 1. ULTRASONIC EVALUATION PROCEDURE PARAMETERS

Measurement	Pre-hydrobuckle	Post-hydrobuckle	GEBS
Instrument Frequency (MHz)	1	1	1
Gast Level (percent loss)	15	15	15
Gain Range Midpoint (dB)	75	85	78
T.T.F. (MHz)	5	5	1
Transmitter Width (in.)	0.5	0.5	0.75
T.R.F. (Mhz)	1	1	1
Receiver Width (in.)	1.0	1.0	0.75

T.T.F. = Transducer Transmitter Frequency
T.R.F. = Transducer Receiver Frequency

TABLE 2. COMPUTED TOMOGRAPHY EVALUATION PROCEDURE PARAMETERS

Investigation	Sample	Plug	Scantime	Circle Size	Slice Width
CCT-Post-Fire	Exitcone assembly	Yes	27.3 sec	480 mm	3 mm
Char Profile	NQ1, NQ2	No	10.8	250	10
SRM	Nozzle Sections	No			
	Tangential		10.8	250	6
	Axial		2.6	410	6
GEBS		Yes	10.8	250	6

TABLE 3. RADIOGRAPHY EVALUATION PROCEDURE PARAMETERS

Investigation	Sample	Facility	Tangential/ Axial/Radial	No. Shots	KeV	mA	Time (min)	ff1* (in.)	Film Type
CCT-1: Pre-Fire	Exit cone assembly	MTI/E	Tan.	each 17°	150	8	2.8	96	D55-D45
			Axial		110	8	1.9	80	D55-D45
	Nozzle assembly	MTI/E	Tan.	each 30°	400	8	1.2	80	D55-D65
CCT-1: Post-Fire	Exit cone assembly	MTI/E	Tan.	each 15°	170	10	2.0	48	R
			Axial	each 90°	150	10	2.0	60	R
CCT-1: Pre-Hydrobuckle	Hydrobuckle segment	MSFC	Tan.	each 30°	50	10	0.75	48	M
			Radial	each 30°	40	7	0.33	48	M
CCT-1: Post-Hydrobuckle	Hydrobuckle segment	MSFC	Radial	each 30°	40	7	0.33	48	m
SRM	9B-404	MSFC	Tan.		70	10	2.0	48	M
			Radial		100	10	2.0	48	M
	9B-403		Tan.		70	10	2.0	48	M
			Radial		75	10	2.0	48	M
	14A-404		Tan.		75	10	2.0	48	M
GEBS			Tan.		70	10	2.0	48	M

* ff1 = film-focal distance

TABLE 4. DATA MAPPING TECHNIQUE SUMMARY

Program	Technique(s) Used	Contributing NDE Method(s)
PAM-D (CCT-1)	Visual data recording	Visual
	Comparative analysis	Visual, radiography (radial, axial, tangential), computed tomography
PAM-D (CCT-1 Aft Section)	Visual data recording	Visual
	Comparative Analysis	Visual, radiography)radial and tangential), ultrasonics, acoustic emissions
Char Profile	Visual data recording	Visual
	Anomaly profiling	Computed tomography
SRM Concerns	Visual	Visual

TABLE 5. CCT-1 NDE EFFORT/OVERVIEW

CCT-1 EXIT CONE ASSEMBLY INVESTIGATION
MSFC 12/24 — 1/2

DATA GENERATED

Macro Photography — 9 total	Every 90° Exterior Every 90° Interior (angled) Direct Along Z Axis
Micro Photography — 11 total	4 Shots-Eroded Edges 1 Shot-Non-Eroded Edge 1 Shot-Delaminated Edge 1 Shot-Large Crack 4 Shots-Interior Regions
X-Rays Taken 16 total	2 Tangential 270° 3 Tangential 110°, 115°, 120° 4 Tangential 60°, 62°, 64°, 66° 5 Tangential 266°, 268°, 270°, 272°, 274° 2 Axial
CCT-Scans 60 total	Mandrel Fabricated Approximately 60 Shots/Scans Taken 33 Scans Hardcopied

DATA REVIEWED

MTI/E — Tangential x-rays mapped for bond gaps, thread gaps, LDI's, anomalies and locations of interest for MSFC review-26 x-rays mapped

ALL (60) — CT Scans reviewed, 33 scans selected for hardcopy, 13 scans selected for mapping (see above) - metal fragments also noted.

Transfer of Tangential x-ray mapping charts to circumferential maps for CT-Scan comparison — 5 locations selected.

Visual Investigation of Assembly — (See Attached).

Micro Photography — Surface cracking noted aft of C/P insulator. Circumferential, evenly spaced lines noted in eroded, non-eroded, main body and aft regions of C/C cone.

APPENDIX A

The information gathered from experimental data (GEBS) was applied toward the establishment of a procedure for calculating relative probabilities of failure. Failure can be induced by many conditions and in many ways. For items with firm, well understond accept/reject criteria, it is possible to accurately predict failure probability. No such criteria have been defined for the GEBS system. Therefore, the NDE analysis of these struts was based on a relative probability of failure assuming a delamination-type failure mode.

Probability of Failure = percent void content/delaminous region X100 total area

Tensile tests are used to provide a measure of the ultimate strength of a material (U), while fatigue tests may measure the time (t) a sample survives repeated loading. In either test, there exists a point (U max or t max) where a given specimen will fail. The relative probabilties presented herein are based upon this assumption. At a defined U nominal the probability of failure of the weakest strut (P weak) is defined as 1.

The NDE predictions for the GEBS investigation defined the weakest strut (greatest total percent delaminous region) was strut 5.

The relative probability presented in Table A-1 further assumes that the failure mechanism is linearly related to the percent delamination.

TABLE A-1

Strut Number	Percent Delamination	Relative Failure Probability
1	0.11	= (0.11/7.72) = 0.014
3	1.22	= 0.158
4	4.16	= 0.437
5	7.72	= 1.000
6	3.10	= 0.402
7	1.94	= 0.251

APPROVAL

COMPUTED TOMOGRAPHY FOR NON-DESTRUCTIVE EVALUATION OF COMPOSITES: APPLICATIONS AND CORRELATIONS

By G. Goldberg, L. Hediger, and E. Noel

The information in this report has been reviewed for technical content. Review of any information concerning Department of Defense or nuclear energy activities or programs has been made by the MSFC Security Classification Officer. This report, in its entirety, has been determined to be unclassified.

E C McKannan for

R. J. SCHWINGHAMER
Director, Materials and Processes Laboratory